Uncertainty Quantification in CFD analyses using Generalised Polynomial Chaos method

A dissertation submitted to The University of Manchester for the degree of Master of Science in Thermal Power and Fluid Engineering in the Faculty of Engineering and Physical Sciences

2016

Pavan Pranjivan Mehta

Student ID: 9638567

School of Mechanical, Aerospace and Civil Engineering

The University of Manchester

Project Supervisor – Dr Imran Afgan

Table of Contents

Word count: 13,883

List of Figures

List of Tables

Abstract

Uncertainty quantification was conducted using non – intrusive form of Generalised Polynomial Chaos methods for square inline tube bundles. The input was treated as uncertain. Uncertainties were considered in Reynolds number of the flow and distance between two tubes of square inline tube bundles, *P/D*. The range were considered as $250 \leq Re \leq 1000$ and $1.5 \leq P/D \leq 5$. The desired gPC output was to determine the lift, drag and skin friction coefficient for the input range. At first the gPC method were validated for a univariate and a multi – variate case, cosine function and spring body problem respectively.

Declaration

I declare that the dissertation this is my original work unless referenced clearly to the contrary, and no portion of the work referred to in the dissertation has been submitted in support of an application for another degree or qualification of this or any other university or other institute of learning.

Intellectual Property Statement

i. The author of this dissertation (including any appendices and/or schedules to this dissertation) owns certain copyright or related rights in it (the "Copyright") and s/he has given The University of Manchester certain rights to use such Copyright, including for administrative purposes.

ii. Copies of this dissertation, either in full or in extracts and whether in hard or electronic copy, may be made only in accordance with the Copyright, Designs and Patents Act 1988 (as amended) and regulations issued under it or, where appropriate, in accordance with licensing agreements which the University has entered into. This page must form part of any such copies made.

iii. The ownership of certain Copyright, patents, designs, trademarks and other intellectual property (the "Intellectual Property") and any reproductions of copyright works in the dissertation, for example graphs and tables ("Reproductions"), which may be described in this dissertation, may not be owned by the author and may be owned by third parties. Such Intellectual Property and Reproductions cannot and must not be made available for use without the prior written permission of the owner(s) of the relevant Intellectual Property and/or Reproductions.

iv. Further information on the conditions under which disclosure, publication and commercialisation of this dissertation, the Copyright and any Intellectual Property and/or Reproductions described in it may take place is available in the University IP Policy, in any relevant Dissertation restriction declarations deposited in the University Library, and The University Library's regulations.

Acknowledgements

I would like to thank Dr. Imran Afgan for providing me extended support for this dissertation. Without which such a topic would have been completed on time. I would also like to thank my parents for always being there for me.

Glossary

gPC – Generalised Polynomial Chaos

SCM – Stochastic Collocation Method

ρ – Density

v – Kinematic viscosity

X – Random variable

$\mathbb{E}[X]$ – Expectation of Random variable *X*

μ_X – Mean of random variable *X*

σ_X – Variance of random variable *X*

a_n - Pochhammer symbol

ξ- Random variable in Hilbert space

Q_p – Quadrature Points

k - Turbulent kinetic energy

ε – Dissipation rate

L/D – Longitudinal pitch to diameter ratio

T/D – Transvers pitch to diameter ratio

P/D – Pitch to diameter ratio

St - Strouhal number

Δt - Time step

y^+ - Non dimensional wall distance

C_L – Lift coefficient

C_D – Drag coefficient

C_F– Skin friction coefficient

CFD – Computational Fluid Dynamics

Chapter 1: Introduction

Uncertainty in any engineering problem arises due to

- Lack of knowledge
- Human errors
- Limits of measurement system or in resources involved

A rudimentary method would be to increase the tolerance of the system making it to be over design. But to economic consideration or a sensitive application, this might not be the best method to employ. Hence, uncertainty quantification becomes an important problem.

To quantify uncertainty a popular and primitive method is the Monte Carlo. But this requires large sampling data, which might not be feasible in problems where generation of data itself is cumbersome. For example, CFD simulations which itself could be computationally intensive. Hence, effective and computationally efficient methods to model and propagate the input uncertainties are necessary for effective development of credible stochastic simulation tools. The discussions here would be a little biased towards problems in modelling flow physics because quantifying uncertainty in CFD was one of the few objectives of this work.

In this research, a nonintrusive or stochastic collocation method of generalised polynomial chaos (gPC) was used to model uncertainties.

The Polynomial chaos method was first brought into prominence by Wiener (1938). Hermite polynomials form the basis for this method and were employed on the basis of Gaussian random variables. Then according to the theorem by Cameron and Martin (1947); such expansions converge for any second-order processes which was primarily governed by the theorem by the authors itself. Xiu and Karniadakis (2003) came up with the concept of generalized polynomial chaos (gPC), which was developed to model the input uncertainty and its propagation in incompressible flow simulations. The formulation of a gPC was done in a probability space.

It could be broadly classified as,

- Intrusive
- Non – Intrusive or Stochastic Collocation Method

1.1 Objective

The objective of the study can briefly said as:

- Writing a FORTRAN code for gPC
- Validation of the code using a univariate and a multi-variate test case
- Obtaining the lift, drag and skin friction coefficients for square inline tube bundles using Star CCM+ at Quadrature points (obtained from gPC pre-processor) and use gPC post processor to obtain the desired results
- Verify the gPC result for square inline tube bundles.

Chapter 2: Literature Review - gPC

2.1 Introduction

For modelling uncertainty by gPC, initially a random variable was used to map the real with the Hilbert space. This random variable, say, *X* was used extensively in the probability space. The gPC was then formulated using the random variable and Hypergeometric class of orthogonal polynomials (*to be discussed in the later part of this work*).

Broadly speaking, gPC can be classified as intrusive and nonintrusive approach; using Galerkin projection or stochastic collocation method respectively which would be discussed in the later sections briefly and then some applications of gPC was dealt toward the end of this chapter.

2.2 Background

Before the formulation of gPC is dealt, some important concepts should be reviewed in this section; namely, Hypergeometric series and some important properties and definition of orthogonal polynomials as well as probability in brief.

2.2.1 Moments, Variance and Expectation of a Random Variable

A Random variable say, *X*, is used to map the real space to probability space. Probability is the measure of likelihood of an event. There are two distributions for a probability, namely, discrete distribution and continuous distribution. A discrete distribution can have jumps, while a continuous distribution doesn't. All the axioms of probability holds true while formulating a gPC.

Moments, variance and expectation is an important feature of random variable. Its description is given in several standard textbooks for probability and also a book on gPC by Xiu (2010).

The mean of a random variable *X* was given by:

$$\mu_X = \mathbb{E}[X] = \int_{\infty}^{-\infty} x f_X(x) dx \tag{2.1}$$

The variance of the random variable *X* was given by:

$$\sigma_X{}^2 = \mathbb{E}[X] = \int_{\infty}^{-\infty} (x - \mu_X)^2 f_X(x) dx \tag{2.2}$$

The *i*th moment of the random variable *X* was given by:

$$\mathbb{E}[X^i] = \int_{\infty}^{-\infty} x^i f_X(x) dx \tag{2.3}$$

For any real function $g(x)$, the expectation of $g(x)$ was given by:

$$\mathbb{E}[g(x)] = \int_{\infty}^{-\infty} g(x) f_X(x) dx \tag{2.4}$$

Often in our study, we use centred moment $\mathbb{E}(X - \mu_X)^2$. The mean, is often regarded as the centre of the random variable *X* or the most likely value of *X*. Standard deviation was given by the square root of the variance. It describes the spread of the random variable *X* around its mean. It can be showed that,

$$\sigma_X{}^2 = \mathbb{E}[X^2] - \mu_X{}^2 \tag{2.5}$$

2.2.2 Orthogonal polynomials

Orthogonal polynomials have been widely studied. Many books have been written on it, to name a few, the books by Szego (1939), Beckmann (1973) and Chihara (1978). In this section some aspects of orthogonal polynomials was dealt from the books mentioned.

Consider $Q_p(x)$ as a *p*th degree polynomial and for a system of polynomials $\{Q_p(x), i \in \eta\}$ with $\eta = \{1,2,3, \dots, N\}$ or $\eta = \{0,1,2,3, \dots, N\}$ for any finite positive integer *N*, then the orthogonal system of polynomials is defined if and only if the following orthogonality relationship is satisfied with respect to a certain real positive quantity ψ

$$\int_M Q_p(x) Q_q(x) d\psi(x) = h_p^2 \, \delta_{pq}, \qquad p, q \in \eta \tag{2.6}$$

where M is the measure of ψ and the h_p are the constants other than zero. If $h_p = 1$ then the system of polynomials become orthonormal.

The measure ψ often associated with a density function $w(x)$ for a continuous case and weights $w(x_i)$ for a discrete case at point x_i. For a continuous case, the relationship given by equation 2.6 then become

$$\int_M Q_p(x)Q_q(x)w(x) = h_p^2 \delta_{pq}, \qquad p, q \in \eta \tag{2.7}$$

And for a discrete case,

$$\sum_{i=0}^{N} Q_p(x_i)Q_q(x_i)w(x_i) = h_p^2 \delta_{pq}, \qquad p, q \in \eta \tag{2.8}$$

where N can also take the value ∞.

$w(x_i)$ and $w(x)$ are known as the weighting functions for a orthogonal polynomial for a continuous and a discrete case respectively.

2.2.3 Hypergeometric series

The Hypergeometric class of orthogonal polynomials was first studied by Askey (1985); and now it is known as the Askey scheme which is named after him. This section reviews some aspects of hypergeometric orthogonal polynomials in brief. For convenience and generality the same notation as of the original work done by Koekoek and Swarttouw (1998) and Schoutens (2000) was followed.

The Pochhammer symbol (a_n) given by

$$(a_n) = \begin{cases} 1 & \text{if } n = 0 \\ a(a+1)(a+2)\dots(a+n-1) & \text{if } n = 1, 2, 3, \dots \end{cases} \tag{2.9}$$

In terms of Gamma function, it is written as,

$$(a_n) = \frac{\Gamma(a+n)}{\Gamma(a)} \quad , \; n > 0 \tag{2.10}$$

Using the above relation, the hypergeometric series *rFs* in general form is given by,

$$rFs(a_1, \dots, a_r \; ; \; b_1, \dots, b_s \; ; z) = \sum_{k=0}^{\infty} \frac{(a_1)_s, \dots, (a_r)_s \, z^k}{(b_1)_k, \dots, (b_r)_k \, k!} \tag{2.11}$$

where $b_i \neq 0, 1, 2, \dots$ for $i = \{1, 2, \dots, s\}$, this condition ensures that the denominator does not become zero. The radius of convergence ρ for the above hypergeometric series is given by,

$$\rho = \begin{cases} \infty, \text{if } r < s+1 \\ 1 \, , \text{if } r = s+1 \\ 0 \, , \text{if } r > s+1 \end{cases} \tag{2.12}$$

2.3 Askey Scheme

Figure 1 was produced by Schoutens (2000), which is the representation of the hypergeometric orthogonal polynomials as a tree structure. The tree begins with Wilson and Racah polynomials, being continuous and discrete respectively. The lines represent the limit relationship between them.

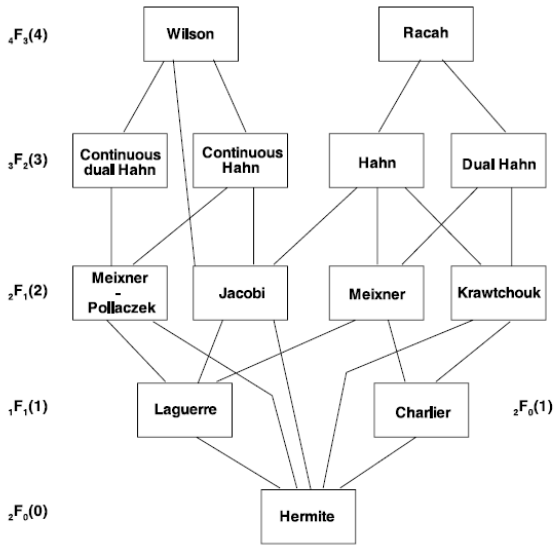

Figure 1: Askey Scheme polynomials relationship by Schoutens (2000)

2.4 Generalised polynomial chaos: Askey chaos

In this section, gPC is formulated. A brief description is given as follows. Wiener (1938) first formulated it using Hermite polynomials. Later on, Xiu and Karniadakis (2003) generalised this approach to all the hypergeometric orthogonal polynomials present in the Askey scheme (figure 1 and figure 2). The term Askey chaos was coined by Xiu and Karniadakis (2003) in their work, here after, it will be used extensively.

As per Xiu and Karniadakis (2003), the second order random process $X(\omega)$ in its general form is given as:

$$\begin{aligned} X(\omega) \quad = \quad & a_0 A_0 \\ & + \sum_{i_1=1}^{\infty} a_{i_1} A_1\left(\xi_{i_1}(\omega)\right) \\ & + \sum_{i_1=1}^{\infty} \sum_{i_2=1}^{i_1} a_{i_1 i_2} A_2\left(\xi_{i_1}(\omega), \xi_{i_2}(\omega)\right) \\ & + \sum_{i_1=1}^{\infty} \sum_{i_2=1}^{i_1} \sum_{i_3=1}^{i_2} a_{i_1 i_2 i_3} A_3\left(\xi_{i_1}(\omega), \xi_{i_2}(\omega), \xi_{i_3}(\omega)\right) + \cdots \end{aligned} \tag{2.16}$$

where $A_n\left(\xi_{i_1}, \ldots, \xi_{i_n}\right)$ denotes the any hypergeometric orthogonal polynomials in the Askey scheme of the *n*th order in terms of the multidimensional variables $\xi = \left(\xi_{i_1}, \ldots, \xi_{i_n}\right)$.

Correspondence of the type of Wiener–Askey polynomial chaos to the type of random inputs ($N \geqslant 0$ is a finite integer)

	Random inputs	Wiener–Askey chaos	Support
Continuous	Gaussian	Hermite-chaos	$(-\infty, \infty)$
	Gamma	Laguerre-chaos	$[0, \infty)$
	Beta	Jacobi-chaos	$[a, b]$
	Uniform	Legendre-chaos	$[a, b]$
Discrete	Poisson	Charlier-chaos	$\{0, 1, 2, \ldots\}$
	Binomial	Krawtchouk-chaos	$\{0, 1, \ldots, N\}$
	Negative binomial	Meixner-chaos	$\{0, 1, 2, \ldots\}$
	Hypergeometric	Hahn-chaos	$\{0, 1, \ldots, N\}$

Figure 2: Types of Wiener - Askey Polynomial chaos (Xiu and Karniadakis, 2003)

For notational convenience Xiu and Karniadakis (2003) rewrote, equation 2.18 as:

$$X(\omega) = \sum_{j=1}^{\infty} \widehat{a_j}\phi_j(\xi) \tag{2.17}$$

As per research conducted by Xiu and Karniadakis (2003); there is a one-to-one correspondence between the functions $A_n(\xi_{i_1}, \dots, \xi_{i_n})$ and $\phi_j(\xi)$, and also their coefficients $\widehat{a_j}$ and $a_{i_1}, \dots, a_{i_n}$.

> Xiu and Karniadakis (2003) stated "… *Since each type of polynomials from the Askey scheme form a complete basis in the Hilbert space determined by their corresponding support, we can expect each type of Askey-chaos to converge to any L_2 functional in the L_2 sense in the corresponding Hilbert functional space as a generalized result of Cameron–Martin theorem, which was presented by Cameron and Martin (1947) and Ogura (1972).*"

The orthogonality relation of the Askey-chaos polynomial chaos can be expressed as:

$$\langle \phi_i \phi_j \rangle = \langle {\phi_j}^2 \rangle \delta_{ij} \tag{2.18}$$

where δ_{ij}, which is the Kronecker delta and $\langle .,. \rangle$ collectively denote the ensemble average which is the inner product in the Hilbert space of the variables ξ.

$$\langle f(\xi)g(\xi) \rangle = \int f(\xi)g(\xi)W(\xi)d\xi \tag{2.19}$$

Or

$$\langle f(\xi)g(\xi) \rangle = \sum_{\zeta} f(\xi)g(\xi)W(\xi)d\xi \tag{2.20}$$

In this case, $W(\xi)$ is presented as the weighting function which corresponds to the Askey polynomials chaos basis $\langle \phi_i \rangle$.

> Xiu and Karniadakis (2003) also stated *"... Some types of orthogonal polynomials from the Askey scheme have weighting functions of the same form as the probability function of certain types of random distributions."*

The original Wiener polynomial chaos, proposed by Wiener (1938) used Hermite polynomials and which is a subset of the Askey scheme can be reproduced by substituting Hermite polynomials $H_n(\xi_{i_1}, \dots, \xi_{i_n})$ in place of $I_n(\xi_{i_1}, \dots, \xi_{i_n})$ in equation 2.16 with the weighting function appearing in equation 2.19 as:

$$W(\xi) = \frac{1}{\sqrt{(2\pi)^n}} \mathrm{e}^{-1/2\xi^T\xi} \tag{2.21}$$

Where *n* is the dimension of ξ.

2.5 Methodology

This section describes the formulation of generalised polynomial chaos in brief. For uncertainty quantification using gPC, there are two approaches, namely, intrusive and non-intrusive. In intrusive approach, the gPC is applied with Galekerian projection and it's applied to the Navier Strokes equations, while the non – intrusive approach used stochastic collocation method. Both these method is discussed briefly in the later parts of this work.

2.5.1 Galerkin Projection

Xiu and Karniadakis (2003) proposed a solution for the Navier–Stokes equations through the usage of a generalized polynomial chaos expansion using Galerkin projection. The resulting solution was expressed in its weak form and formed part of an approach which was the intrusive form of gPC.

This approach discussed in brief by taking the incompressible Navier strokes equation which is given as:

$$\nabla . \mathbf{u} = 0 \tag{2.22}$$

$$\frac{\partial \mathbf{u}}{\partial t} + (\mathbf{u}.\nabla)\mathbf{u} = -\nabla \Pi + Re^{-1}\nabla^2 \mathbf{u} \tag{2.23}$$

where the pressure is represented by Π and the Reynolds number by *Re*. The definition of stochastic processes is applied to all flow quantities. Research conducted by Xiu and Karniadakis (2003) brought to the forefront a random dimension which has been introduced in addition to the spatial–temporal dimensions *(x, t)*, denoted by the parameter ω, thus,

$$\mathbf{u} = \mathbf{u}(\mathrm{x}, t; \omega); \qquad \Pi = \Pi(\mathrm{x}, t; \omega) \tag{2.24}$$

Applying the generalised polynomial chaos expansion, from equation 2.17, we get,

$$\mathbf{u}(\mathrm{x}, t; \omega) = \sum_{i=0}^{P} \mathbf{u}_i(\mathrm{x}, t)\phi_i(\xi(\omega)); \tag{2.25}$$

$$\Pi(\mathrm{x}, t; \omega) = \sum_{i=0}^{P} \Pi_i(\mathrm{x}, t)\phi_i(\xi(\omega)); \tag{2.26}$$

where the infinite summation in infinite dimension of ξ in equation 2.20 has been replaced by a truncated finite-term summation in finite dimensional space of ξ. As per the work done by Ghanem and Spanos (1991), the number of random dimensions (*n*) of ξ and the highest order (*p*) of the polynomials ϕ have a bearing on the total number of expansion terms, *(P + 1)*.

$$P = \sum_{s=0}^{P} \frac{1}{s!} \prod_{r=0}^{s-1} (n + r) \tag{2.27}$$

Xiu and Karniadakis (2003) later stated, "… *The most important aspect of the above expansion is that the random processes have been decomposed into a set of deterministic functions in the spatial temporal variables multiplied by the random basis polynomials which are independent of these variables."*

Then Xiu and Karniadakis (2003), substituted equations 2.25 and 2.26 into Navier–Stokes equations 2.22 and 2.23 as a way of noting the consideration of partial derivatives in a physical space and their interaction with the operations in random space, we end up obtaining the following equations:

$$\sum_{i=0}^{P} \mathbf{u}_i(\mathrm{x}, t)\phi_i = 0, \tag{2.28}$$

$$\sum_{i=0}^{P} \frac{\partial \mathbf{u}_i(\mathrm{x}, t)}{\partial t}\phi_i + \sum_{i=0}^{P}\sum_{j=0}^{P} [(\mathbf{u}_i.\nabla)\mathbf{u}_j)]\,\phi_i\phi_j = -\sum_{i=0}^{P} \nabla \Pi_i(\mathrm{x}, t)\phi_i + Re^{-1}\sum_{i=0}^{P} \nabla^2 \mathbf{u}_i\phi_i \tag{2.29}$$

The equations arrived at above have further been projected into the random space spanned by the basis polynomials $\{\phi_i\}$ by taking into consideration the inner product of above equation with each basis polynomial. The following set of equations has been derived through the utilization of the orthogonality condition coupled with taking into consideration the $\langle ., \phi_k \rangle$. :

For each $k = 0; \ldots ; P$,

$$\nabla . \mathrm{u}_k = 0, \tag{2.30}$$

$$\frac{\partial \mathbf{u}_k}{\partial t} + \frac{1}{\langle {\phi_k}^2 \rangle}\sum_{i=0}^{P}\sum_{j=0}^{P} e_{ijk}[(\mathbf{u}_i.\nabla)\mathbf{u}_j)] = -\nabla \Pi_k + Re^{-1}\nabla^2 \mathbf{u}_k \tag{2.31}$$

where $e_{ijk} = \langle \phi_i \phi_j \phi_k \rangle$. The definition of ϕ_i, along with $\langle {\phi_i}^2 \rangle$ can be studied analytically to evaluate the coefficient e_{ijk}. The *(P + 1)* system of Navier–Stokes-like equations for each random mode coupled through the convective terms is used in the formation of the concerned set of equations.

2.5.2 Stochastic collocation method

Stochastic collocation method is a non-intrusive approach. Unlike the Galerkin approach, this method was straight forward as it evaluates statistical moments by sampling the solver at a finite number of deterministic points within Γ. In the form of a spectral representation of the stochastic solution, this method is highly accurate, as simple as the Monte Carlo method, and consequently highly advantageous.

There two major approaches for higher – order for higher order stochastic collocation, namely, interpolation approach and the discrete projection or pseudo-spectral approach. Forthis work, the pseud- spectral approach esd. Hence, the interpolation approach introduced is not dealt here.

2.5.2.1 Discrete Projection: Pseudo-spectral Approach

The discussion of discrete projection is largely based on the work done by Xiu (2007) and also it's well written in a book by Xiu (2010). However, this method and the above method is greatly discussed and formulated in many literatures dealing with uncertainty quantification using gPC for specific problems and in some cases for a range of problems. Some of them will be discussed in the later sections of this work, which mainly deal with its application.

2.5.2.1.1 Formulation

The term *cubature rule* which is an *integration rule* used to approximate on integral in a multivariate space. It can be considered as an extension of the *quadrature rule* in multivariate space, in contrast of it being used in a univariate space.

In order to formulate the discrete projection, let's recall the exact orthogonal gPC projection from (equation 2.17)

$$X(\omega) = \sum_{j=1}^{\infty} \widehat{a_j}\phi_j(\xi) \tag{2.32}$$

and the expansion coefficients $\widehat{a_j}$ are evaluated as follows,

$$\widehat{a_j} = \frac{1}{\gamma_j}\mathbb{E}\left[a_j(\xi)\phi_j(\xi)\right] = \frac{1}{\gamma_j}\int a_j(\xi)\phi_j(\xi)d(\xi),\ \ \forall|j| \leq N \tag{2.33}$$

and $\gamma_j = \mathbb{E}[{\phi_j}^2]$ are the normalization constant.

The ideology behind it is to approximate the integrals in the expansion coefficients' of equation 2.33 of a continuous gPC projection by cubature rule.

The formulation of gPC by expanding equation 2.32 and 2.33 can also be considered as a post processing step after all the computations are finished at the cubature nodes. In this method, the coefficients are evaluated only at important computational points for a given problem without evaluating the all the coefficients. Such is the case when global sensitivity is necessary for some random variable. While the gPC Galerkin Method requires to compute all the gPC coefficients which are coupled and solved simultaneously.

2.5.2.2 Structured Nodes: Tensor and Sparse Tensor Constructions

As the Gauss Quadrature rules our highly accurate for univariate integration, hence it is reasonably enough to extend the idea to multivariate integration. The straightforward method is to construct high order integration rules of the quadrature rules to high dimensional spaces by using tensor constructions.

Even though this method can be easily constructed as well as it is highly accurate, the underlining problem here was the rapid growth of the total number of points in high dimensional random spaces. For example, if equal number of nodes is taken in all directions, say *n* number of nodes then the total number of nodes is the power of *n*,

which can be quite large as n is a positive number much greater than 1. Hence, this approach is usually used for $n < 6$.

2.5.2.3 Non Structured Nodes: Cubature

Cubature rules are still being studied actively, in spite of its oldness. A high degree of polynomial exactness and a lesser number of nodes is achieved by using a cubature rule. In order to achieve this, majority of studies find their basis in geometric considerations. Furthermore, structured nodes are not taken into consideration. An explicit formula is majorly used when talking about node locations and their corresponding weights. The choice of a proper cubature with an affordable number of nodes for simulations was dependent upon the required accuracy for the discrete gPC approach. The collections of available cubature rules can be reviewed extensively in work done by Cools (2003), Stroud (1971) and Haber (1970).

Moreover, it must be kept in mind that cubature rules do not require the classical error estimation in terms of error bounds, for their operation. Additionally, polynomial exactness plays a crucial role in classifying the accuracy of cubature rules.

2.6 Applications of gPC

Uncertainty quantification using gPC has been widely used for a number of applications; some of them are discussed below:

2.6.1 Incompressible flow

Han *et al* (2012), studied for a two dimensional flow over a flat plate in laminar flow regime. The uncertainty was introduced in the inflow conditions; both the Reynolds number and angle of incidence were used as uncertain parameters which were modelled using random variables. Nonlinear coupling between the two uncertainties was also studied by them. Standard deterministic numerical simulation was coupled with gPC.

Le Maiter *et al.* (2001) conducted their study for an incompressible fluid in laminar flow region at moderate Reynolds number for a two dimensional channel using gPC

Galerkin projection. In his study he chose inflow velocity as uniform and also considered no-slip wall condition. The Reynolds number chosen was *Re* = 81 and it was solved for steady and laminar case. In his case he modelled the the viscosity as a Gaussian ramdom variable. Xiu and Karniadakis (2003) modelled incompressible flow channel and the second case under their investigation was modelling flow around a circular cylinder. They modelled the flow using gPC Galerkin projection.

Narayanan and Zabaras (2005) used a global approach, which is non-intrusive gPC method; also referred to as stochastic collocation method for stabilized FEM solutions for a flow in a channel and a cavity using an incompressible fluid. Le Maitre (2006) investigated inviscid incompressible flow around an aerofoil using an intrusive or Galerkin approach of the gPC. Le Maitre and Knio (2007), for an incompressible flow computation using gPC, they introduced stochastic particle-mesh vortex method.

Lucor *et al*. (2007) studied the sensitivity of LES (large eddy simulation) statistical moments to parametric uncertainty in the sub grid scale model for decaying homogeneous isotropic turbulence. They used both intrusive and non-intrusive gPC approach. For the spectral collocation method they used non statistical numerical methods which are well suited for Gaussian variables. For different resolution in the grid, they conducted their analysis at *Re* = 100. The results of gPC are also compared to Direct Numerical Simulation. They also showed that for the solution responded differently for different turbulent scales of LES

2.6.2 Compressible flow

Computing compressible flow using gPC is a challenge as there are shocks in such flows, which leads to discontinuity in our solution as well as in all our flow properties.

This challenge has motivated several authors to tackle the problem. One such example is the work done by Chen *et al*. (2005), they has extensively discussed about it. In his work, they used an intrusive gPC approach for uncertainty quantification. A nonlinear inviscid Burgers equation model for a steady-state isentropic nozzle flow was studied by them. The uncertainty was introduced in the form of initial conditions and shock

location. The outcome of their work showed, even though there exit a discontinuity across the shock in terms of velocity, the gPC dependence was rather smooth. They also indicated that there were problems with the convergence of the gPC as there was a discontinuity across the shock, to tackle this problem; they introduced filtering as a necessary condition for numerical stability. They also observed, for a low level of uncertainty in initial condition predicted the uncertain shock location accurately, while for high level of uncertainty in initial condition the convergence was rather slow as it required solving many terms.

Apart for the shocks in compressible flow, another flow feature possess a challenge in compressible flow, is the Prandtl – Meyer expansion wave. This motivated Perez and Walters (2005) to study flow over a wedge (shock affected region) and over an expanding corner (Prandtl – Meyer expansion wave affected region). They employed an intrusive gPC method. Lin *et al.* (2006), also studied the supersonic flow. In their work they modelled flow over a wedge, they employed intrusive gPC and ME-gPC approach.

Hosder et al. (2006) also took the challenge of solving the compressible flow problem. Their work compared the nonintrusive or spectral collocation method of the gPC with the Monte Carlo method of quantifying uncertainty. They discovered that, for a flow around a wedge, mostly the non – Gaussian statistics were able to predict the location of shock, where it required using a high order polynomial to reduce the error. While, for the expansion wave problem, the Gaussian statistics were sufficient enough and achieved small errors. Later on, Hosder *et al.* (2008) extended the work and used the scheme developed for uncertainty quantification for a flow around a transonic wing.

Mathelin *et al.* (2004) investigated a case of turbulent supersonic quasi 1D nozzle flow using an intrusive gPC approach. The nonlinearity and discontinuity in formulating the intrusive form of gPC, led Mathelin and Hussaini's (2003) to develop a non-intrusive stochastic collocation method. This was achieved by constructing it for a stochastic Riemann problem which has a discontinuity in the variables representing flow quantities as it has a shock wave and an expansion fan. They used this scheme to construct gPC for turbulent supersonic quasi 1D nozzle flow and

demonstrated its accuracy and computational efficiency. They also compared this solution to Monte Carlo method of uncertainty quantification.

2.7 Conclusion

The description about the differences in gPC approaches is well explained by Xiu (2010). The ease in implementation is the biggest advantage of stochastic collocation. Additionally, it has very straightforward algorithms which have been listed below and also aligned in figure 3.

1. Multivariate interpolation theory or integration theory should be used as basis for choosing an appropriate set of nodes.
2. A deterministic code must be applied at each node.
3. gPC polynomials should be constructed using a post process mechanism by using any one of the interpolation approach or the discrete projection approach.

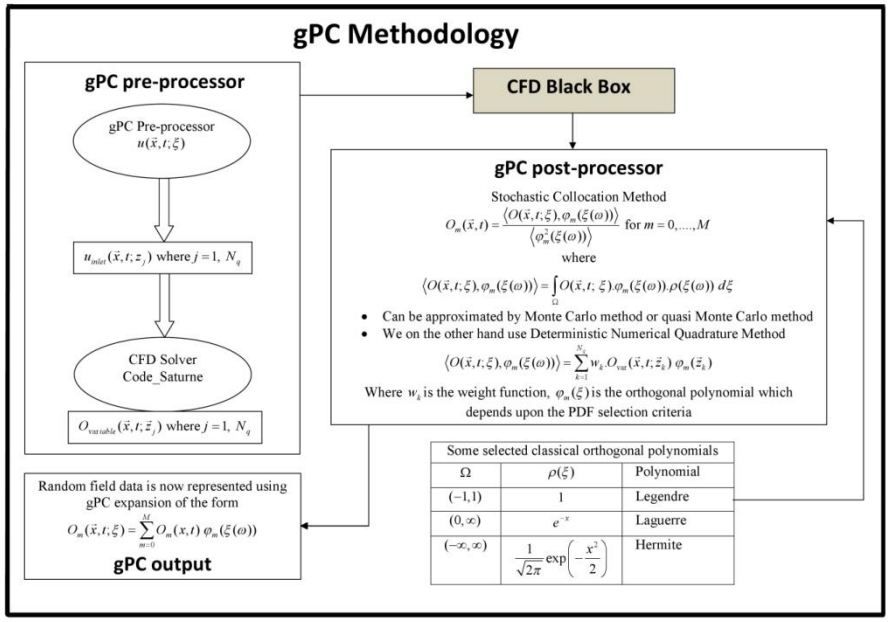

Figure 3: gPC Spectral collocation methodology ***(according to the communications with Dr. I. Afgan, University of Manchester)***

An original problem, and its complexity and nonlinearity does not affect the functionality of the stochastic collocation as long as a reliable deterministic solver can be developed. The executions of the deterministic algorithm were extremely parallel to one another and additionally, they were completely independent of each other. These were the prime reasons behind the increasing popularity of stochastic collocation methods.

In comparison, the implementation of the stochastic Galerkin method is a lot more challenging. A derivation of the Galerkin system must be obtained, whose expansion coefficients are coupled with a high frequency. Consequently, larger, coupled system of equations needs to be dealt with through the development of new codes. The highly complex and nonlinear form of the original problem can render the explicit derivation of the gPC equations nontrivial and sometimes even impossible.

Chapter 3: gPC test functions

3.1 Introduction

This chapter attempts to validate the FORTRAN code written for non – intrusive Generalised polynomial Chaos (gPC) by using analytical test functions.

The notation followed throughout the chapter were, *Qp* for Quadrature Points, SCM for Stochastic Collocation method and gPC for non – intrusive Generalised polynomial Chaos. It is to be noted gPC and SCM imply the same thing, hence were used interchangeably.

3.2 Legendre Polynomials

Legendre polynomials were orthogonal polynomials in the Askey scheme. Like any other orthogonal polynomial, they also satisfy orthogonality and can be subsequent order of polynomial can be generated by using the pervious polynomial of the same class (as discussed in the previous chapter). The first few polynomials are,

$$f_0(x) = 1 \tag{3.1}$$

$$f_1(x) = x \tag{3.2}$$

$$f_2(x) = \frac{1}{2}(3x^2 - 1) \tag{3.3}$$

$$f_3(x) = \frac{1}{2}(5x^3 - 3x) \tag{3.4}$$

$$f_4(x) = \frac{1}{8}(35x^4 - 30x^2 + 3) \tag{3.5}$$

where the subscript of function, f denotes the polynomial order. For Legendre polynomials to be orthogonal a necessary condition was given by,

$$-1 \leq x \leq 1 \tag{3.6}$$

This imposes a necessary condition on the random variable, ξ in the Hilbert space in any dimension as follows,

$$-1 \leq \xi \leq 1 \tag{3.7}$$

Transformations from the real space to Hilbert space were done in-order to satisfy equation 3.7. Before writing the complete code in FORTRAN for the gPC pre – processor, Legendre polynomials were obtained and validated. Equation 3.6 should be satisfied at all times and interestingly enough for any given order, the range of $f_i(x)$ is also [-1, 1], where $i \in [0, \infty)$. Figure 4, was the resulting output for different orders of Legendre polynomials for a univariate case.

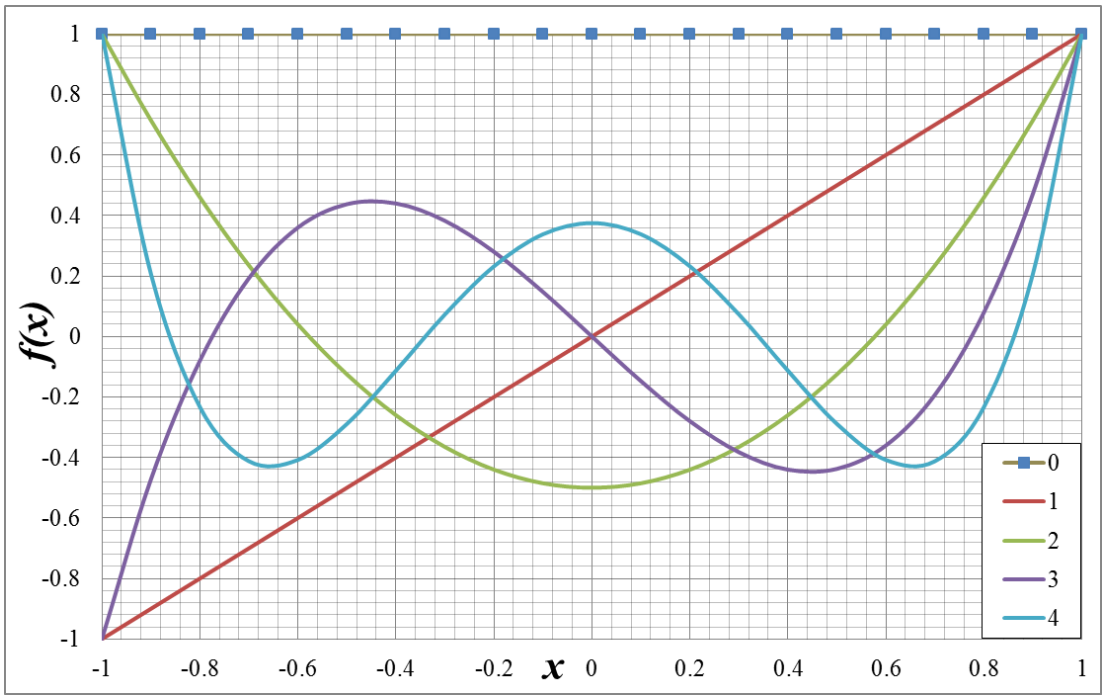

Figure 4: Legendre Polynomials of different order.

For a multi-variate case, this idea is extended and a hyper cube of [-1, 1] ^{d} is obtained, where d is the number of dimensions, $d \in \mathbb{N}$.

3.3 Univariate test case

The test case presented in this section aims to determine the number of Quadrature Points required to approximate a given test function with sufficient accuracy. Hence, the total number of quadrature points was chosen as 2, 4, 6, 8 and 20.

The test function used for it is given as follows,

$$f(x) = \cos(x) \tag{3.8}$$

In equation 3.8, *x* denotes the variable in the real space which was mapped to the Hilbert space. As the test function was periodic in nature, *x* was varied along its period, as,

$$0 \leq x \leq 2\pi \tag{3.9}$$

The following transformation was done between the real and the Hilbert space, where ξ denotes the random variable in Hilbert space.

$$x_i = \frac{x_n + x_0}{2} + \frac{x_n - x_0}{2}\xi_i \tag{3.10}$$

In equation 3.10, x_0 and x_n were the first and last value of *x* for the considered range and $x_n > x_0$.

3.3.1 Pre & post processing

The gPC pre-processor computes the Quadrature points based on the number of points required for accuracy. The code was written in such a way, that the number of Quadrature points was equal to the maximum order of the Legendre polynomial. However, for integral approximations done using Gaussian quadrature rule; have no such requirement as it can use a suitable weighting function based on the points chosen. The independency of selection of computational points and good accuracy makes Gauss Quadrature a popular choice for integral approximation. The prime reason for selecting the polynomial order same as the number of Quadrature Points

was, orthogonal polynomials were known to give very good accuracy if the Quadrature points were the roots of the particular orthogonal polynomial. This implies *n*th order of polynomial having *n* number of roots was best to approximate a given function using *n* Quadrature points.

n	Quadrature points
2	Quad(1) = 1.3288498813483121 Quad(2) = 4.9593351186516887
4	Quad(1) = 0.4366002634468673 Quad(2) = 2.0751606327561287 Quad(3) = 4.2130243672438716 Quad(4) = 5.8515847365531330
6	Quad(1) = 0.2123221788462994 Quad(2) = 1.0651889704810085 Quad(3) = 2.3938516835658628 Quad(4) = 3.8943333164341376 Quad(5) = 5.2229960295189919 Quad(6) = 6.0758628211537005
8	Quad(1) = 0.1248524290266633 Quad(2) = 0.6392993230655790 Quad(3) = 1.4917699457801878 Quad(4) = 2.5673570385961981 Quad(5) = 3.7208279614038022 Quad(6) = 4.7964150542198123 Quad(7) = 5.6488856769344213 Quad(8) = 6.1633325709733366
20	Quad(1) = 2.1604324321597979E-02 Quad(2) = 0.1132756385634841 Quad(3) = 0.2759430844029787 Quad(4) = 0.5058310633380709 Quad(5) = 0.7975558758717778 Quad(6) = 1.1442808907958866 Quad(7) = 1.5378793979778886

	Quad(8) = 1.9691259463304283
	Quad(9) = 2.4279127000167220
	Quad(10) = 2.9034860341277722
	Quad(11) = 3.3846989658722282
	Quad(12) = 3.8602722999832784
	Quad(13) = 4.3190590536695721
	Quad(14) = 4.7503056020221113
	Quad(15) = 5.1439041092041133
	Quad(16) = 5.4906291241282226
	Quad(17) = 5.7823539366619290
	Quad(18) = 6.0122419155970217
	Quad(19) = 6.1749093614365158
	Quad(20) = 6.2665806756784024

Table 1: Quadrature Points for *n*th order

Table 1, provides the Quadrature points for n = 2, 4, 6, 8 and 20. The analytical value of the function (Equation 3.8) was explicitly evaluated at these Quadrature points and used in the gPC post – processor. In general, the values are first determined by either experimentation or using numerical methods and fed to the gPC post – processor.

The gPC post – processor then uses the above values to compute its coefficients when Galerkin Projection was performed. Using these newly obtained coefficients, the second important step it performs was to evaluate the values of the function by series of summation applied to the product of the coefficients and the orthogonal polynomial under consideration (in this case Legendre polynomials) up to the *n*th order was achieved in Hilbert space with a suitable step size to for a tensor gird which gives the values for the entire range (Equation 3.7). Transformations were then carried out to map the Hilbert space to the real space.

3.3.2 Results & discussion

To determine the accuracy and solution behaviour's dependence on the number of Quadrature points used. The solution of gPC was compared to the analytical solution as well as to each other.

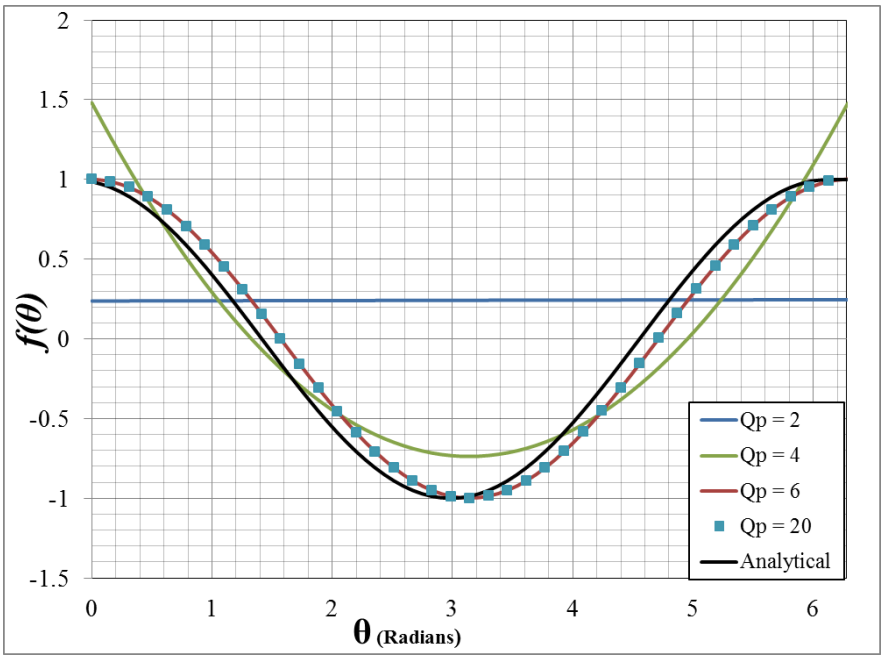

Figure 5: gPC result for different number of Quadrature points in real space

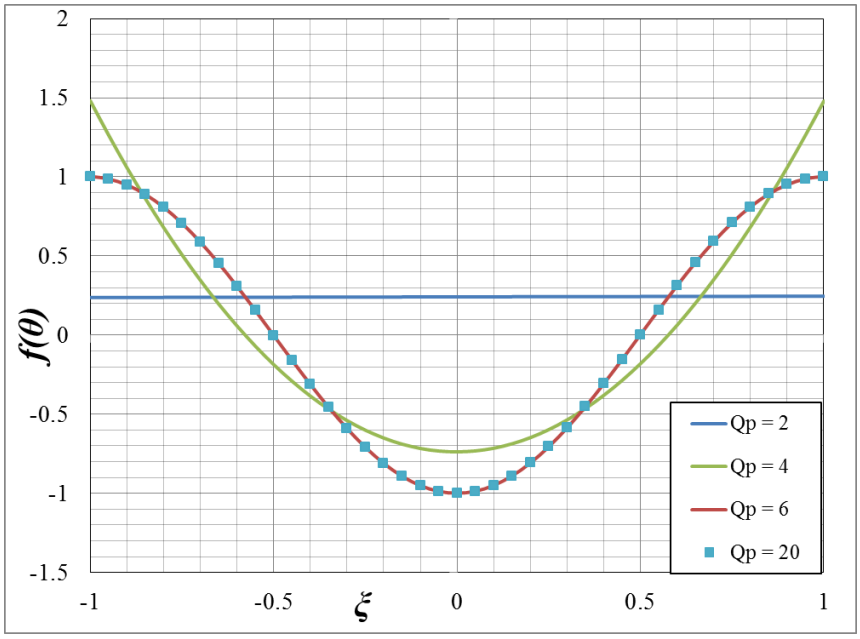

Figure 6: gPC result for different number of Quadrature points in Hilbert space

Figure 5 and Figure 6 was the result obtained by gPC, the data was represented in real and Hilbert space respectively for different choice of number of Quadrature points (*Qp*). Note that on the Y – axis of both the graph have the functional value in real space. This was because the gPC returns values as per the data fed and the subsequent trend in the variation were found accurately irrespective of its magnitude. As in this case the values evaluated were at the Quadrature points in the real space, and not Hilbert space, the return of values was in the real space. If the input values to the post – processor were fed at Quadrature points located in Hilbert Space, the output would be in accordance to the Hilbert space and transformation would be required to bring the values to the real space, rather than readily using the output. This suggests the robustness of the method employed and proves that irrespective of the data in either Hilbert or Real space, the numerics of this method were independent of the choice of space. However, in the pre – processing the same was not true as the first step was to evaluate the Quadrature points and it was largely dependent on the choice of the orthogonal polynomial. For this case, Legendre Polynomials which had a support of [-1, 1], hence, transformation became a necessary step as the real space exceeded well beyond the limits of Legendre polynomials. However, if the Real space would have limits of [-1, 1] or any other orthogonal polynomial from the Askey scheme was to be used which supports well beyond the limits of Legendre polynomials, for example, Hermite polynomials which has a support of $(-\infty,\infty)$. The transformation wouldn't be required as the two spaces now coincide with each other.

For a multivariate, the above discussion also holds true. However, it would be a bit cumbersome to track the each random variable in each dimension. As the total number of the Quadrature points required could be high enough and given as,

$$Q_m \times Q_n \times Q_o \times Q_p \ \ldots \tag{3.11}$$

where, the *Q* is the number of Quadrature points in *m, n, o, p* … dimension. If there were equal number of Quadrature points in each dimension, then the total number of Quadrature points required would be $Q^{\,d}$, where *d* is the total number of dimensions. Hence, it can be seen as the dimension increase the required of the Quadrature points rises to the power of the dimension, this is commonly referred to as the '*curse of dimensionality*' in literatures over gPC employing Stochastic collocation method (SCM).

Hence it is recommended to first performing the transformation and feed the post processor, the values evaluated at the Quadrature points of real space. This result in output being in real space and complex transformation could be avoided.

Again referring to Figure 5 and Figure 6, it was seen that for the choice of six Quadrature points (*Qp*) or higher the solution remains the same and provided good approximation for the function by capturing the non – linearity accurately, also it was quite close to the analytical solution of the function. The failure of *Qp* = 2 and *Qp* = 4 in an obvious manner suggests they were inadequate to capture the non – linearity. The question is, '*where did they go wrong?*' To address this issue, observe the pattern of the Quadrature points returned by the pre – processor. The points were symmetrically distributed about the mean of its range and also notice the intersection of these curves with *Qp* = 6 or 20. The intersection points are of immediate interest. The points of intersection were the points where they were analytical computed and fed in the post – processor. For *Qp* = 2's (also *Qp* = 4's) intersection with *Qp* = 6 or 20; it has returned the same value at those points as of analytical solution or the solution at respective intersections. In general, insufficiency of the data led to inaccurate results.

For a two point choice of Quadrature; as they were symmetrical distributed about the mean of its range and cosine being an even periodic function has also the same values about the mean of the considered range. Hence, it returned the same value at both of these locations. It is impossible to predict a non – linear curve using only two points. Hence, gPC joined the two points and a straight line was formed. As the values of the cosine function was the same at both of these points. The line became parallel to the X – axis and was offset by the value of the function at those location. It may be a good approximation, only if, it was used to evaluate the values with a linear variation of properties. Therefore, it can be said, for a known linear approximation, choice of *Qp* = 2 would be still valid.

For *Qp* = 4, it has captured the non – linearity, however, it still over predicts the results. At certain locations the results were exceeding the range [-1, 1], which were quite unphysical as cosine function stays between theses limits. It was observed that the point of minima wasn't fed and also there were no Quadrature points when the gradient changed its sign, which wasn't the case for *Qp* = 6 and *Qp* = 20. In a

nutshell, for gPC to give satisfactory results, certain considerations should be under taken while making a choice of number of Quadrature points,

- There should be at least one Quadrature point near or at the minima or maxima of a function.
- There should be at least one Quadrature point immediate before and after the point where the gradient changes its sign.
- If the function or the variation of a certain property is unknown, then running the same experiment with gradual increase of the number of Quadrature points and making suitable comparisons should be a good practise before coming to any conclusion.

The results of Qp = 8, were not shown in the above figures as the gPC returned the values with sufficient accuracy for $Qp \geq 6$ and would overlap, thereby reducing the visibility of the other curves.

3.4 Multi-variate test case

Multi – variate gPC are nothing but mere extensions of univariate gPC method. All conclusions drawn for a univariate case also apply to a multi – variate problem. A simple example was used to validate the code the FORTRAN code with random variables two variables.

A spring mass system was considered. The only degree of freedom was allowed, motion along the X – direction over the horizontal surface. For the sake of validation, the friction between the horizontal surface and the body was assumed to be zero. The spring had a spring constant, k = 9 N/m and mass of the body (m) was taken to be 1 kg. The spring was displaced by a distance of 0.01m and released from rest at time t = 0. The problem statement was to find the subsequent motion of the body, up to 2s and if the initial displacement was unknown but it was given as between 0.01m – 0.1m (both values inclusive). For such a case determine the motion for the same time range.

3.4.1 Pre & post processing

To solve this problem, the uncertainty were considered to be in both time and initial displacement as,

$$0 \leq t \leq 2$$
$$0.01 \leq d \leq 0.1 \tag{3.12}$$

where *d* was the initial displacement. The transformation to Hilbert space was carried out with accordance to equation 3.10 for both time and initial displacement, by considering two random variable ξ_1 and ξ_2, which vary according to equation 3.7 as in this case as well Legendre polynomials were used for uncertainty quantification. One to one correspondence maps the random variable to real and Hilbert space.

The displacement as a function of time after applying the necessary boundary conditions reduces to,

$$x(t) = d.cos(\omega_0.t) \tag{3.13}$$

where $\omega_0 = \sqrt{\frac{k}{m}} = 3 \text{ rad/s}$

Hence the above equation reduces to,

$$x(t) = d.cos(3.t) \tag{3.14}$$

In the above equation 3.14, both *d* and *t* were uncertain and were given as Equation 3.12.

The first step as seen in the previous sections was to determine the Quadrature Points. Six Quadrature points were found in each dimension as it was demonstrated in the previous section the minimum number of six Quadrature Points provided sufficient accuracy, this serves as a good starting point for our validation. The six Quadrature

points generates 36 points for analytical solution of the above equation listed in Table 2.

Quadrature points for time	Quadrature points for displacement
Q_t(1) = 6.7530512809753418E-02	Q_d(1) = 1.3038873076438896E-02
Q_t(2) = 0.3387905955314636	Q_d(2) = 2.5245576798915859E-02
Q_t(3) = 0.7613808065652847	Q_d(3) = 4.4262136295437814E-02
Q_t(4) = 1.2386191934347153	Q_d(4) = 6.5737863704562194E-02
Q_t(5) = 1.6612094044685364	Q_d(5) = 8.4754423201084145E-02
Q_t(6) = 9324694871902466	Q_d(6) = 9.6961126923561097E-02

Table 2: Quadrature points for time and displacement

3.4.2 Results and Discussion

The post processing was performed as the previous univariate case with the modification of the FORTRAN code to accommodate two variables. However, the general idea still remains the same as discussed in the previous section. The contour plot presented was made in Tec plot.

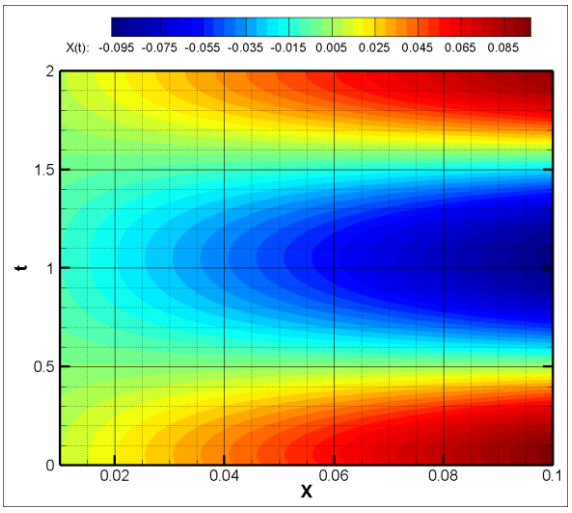

Figure 7: gPC plot in Real space

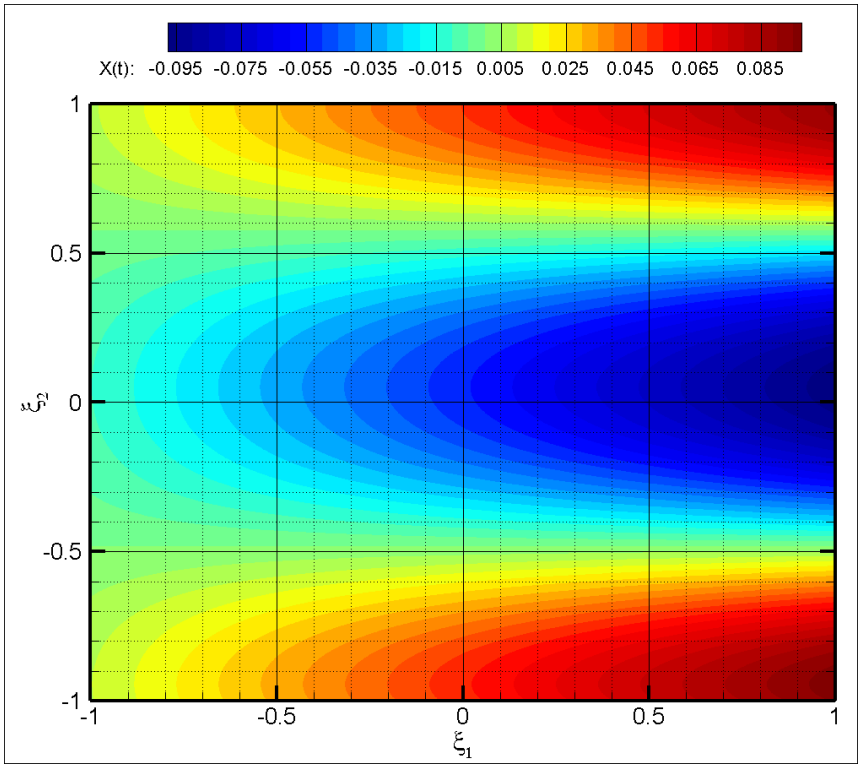

Figure 8: gPC plot in Hilbert space

Figure 7 and Figure 8 represents the values of the function evaluated in real and Hilbert space respectively.

Result	X	t	X(t)
gPC	0.04	1	- 0.045
Analytical	0.04	1	-0.03959

Table 3: Function values

Referring from

Table 3, the values obtained by gPC and Analytical were not much different from each other. From the univariate case it was seen gPC gave quite accurate results. This implies that the discrepancies in the two result occurred due to representation of the gPC result in a contour plot. Because the contour plot groups & averages data before giving a final output. Without a doubt there could be human error in reading the plot.

3.5 Conclusion

The gPC FORTRAN code was validated and following conclusions were drawn,

- Number of Quadrature points used has influence in final output, but after the gPC solution has accurately captured the physics of the problem, further increasing the number of Quadrature points have little or no effect on accuracy.
- Six quadrature points in a given dimension; capture the physics of the problem reasonably well as seen in both; univariate and multivariate case.
- Inadequate representation of the gPC result may lead to high errors.

Chapter 4: Literature Survey – Tube Bundles

4.1 Introduction

Tube bundles are of great practical importance when it comes to heat exchanger design. They have gained popularity because of its simplicity in design, high heat transfer rates and ease in manufacturing. However, the cross-flow over a tube bundle is not that all simple. Hence, this chapter objective is to conduct a literature survey in relation to cross flow in tube bundles.

The pitch (P) is the distance between the centres of the two adjacent cylinders. This distance is non – dimensionalised using the tube diameter (D) as P/D, also known as the gap ratio or spacing between the cylinders. This terminology was used inter-changeably during writing of this chapter as they all mean the same.

The distance can be in two directions, namely, transverse (T) and longitudinal (L), which is perpendicular and along the initial flow velocity respectively. The purpose of this entire work was to conduct uncertainty quantification in square inline tube bundles. This implies the longitudinal and transverse distances are equal. Therefore, P/D was used to represent whenever the two distances were equal, forming a square tube bundle or otherwise explicitly mentioned.

4.2 Single cylinder

Before moving to the discussion of relevant parameters and flow structures for tube bundles. The author of this work wishes to introduce some aspects of single cylinder, in-order to draw suitable conclusions and contrast between a single cylinder and multiple cylinders arrangement. However, this sub section will only deal with qualitative aspects such as flow patterns.

There are different flow patterns observed around a single cylinder. These flow patterns are purely depended on the Reynolds number of the flow. For a flow with $Re < 1$, laminar boundary layer is observed. This boundary layer increase in thickness around the cylinder downstream until separation occurs near the rear stagnation point.

It is to be noted at such low Reynolds number, the inertial forces become negligibly small and the flow is governed by viscous forces.

Recirculation behind the cylinder is observed for higher Reynolds number. For *Re* > 5, two symmetrical vortices are seen. For *Re* > 40, vortex shedding in the rear of the cylinder is a key feature of the flow, because in a structure a resonance condition achieved may sometime lead to catastrophic failure of the structure. These vortices shed periodic in nature and are known as *Von Kármán-Bénard* vortex sheet. If the Reynolds number is further increased, for *Re* > 150, irregular vortices are formed. Small vortices now start to shed with the large ones.

Further increases in Reynolds number leads to enter the sub critical region, which is the flow regime for Reynolds number between from 1000 to 2 x 10^5. In this flow regime, laminar wake followed by turbulent wake further downstream. Regular vortex shedding is observed in this flow regime. On further increase in Reynolds number beyond the critical value, the flow now is fully turbulent in this flow regime, causing the separation point to shift further downstream.

4.3 Flow Pattern

Sumner et al. (1999) reported various flow structures form the experimental study performed on two and three cylinders arrangement. The Reynolds number range of the flow was from 500 to 3,000. The *T/D* was varied from 1 to 6. The above mentioned author categorised three flow regimes described by Reynolds number range and based on the flow pattern observed. The regimes are namely, small for *T/D* < 1.2, intermediate for *T/D* range from 1.2 to 2.2 and large for *T/D* > 2.2. An asymmetry in flow pattern was observed for intermediate region. Kim & Durbin (1988) reported a biased flow pattern and noticed it switches between the two adjacent cylinders. The above mentioned authors described such a phenomenon as bi-stable and found its independency from the Reynolds number of the flow. Sumner et al. (1999) further contributed for such flow behaviour. The authors concluded that the deflection of the flow reduces with increase in *T/D* as seen in figure 9. For a three by three cylinder arrangement a similar flow pattern was observed by Zdravkovich & Stonebanks (1990) as described above and was termed as meta-stable. It was found by the mentioned authors that flow switched its direction with respect to time.

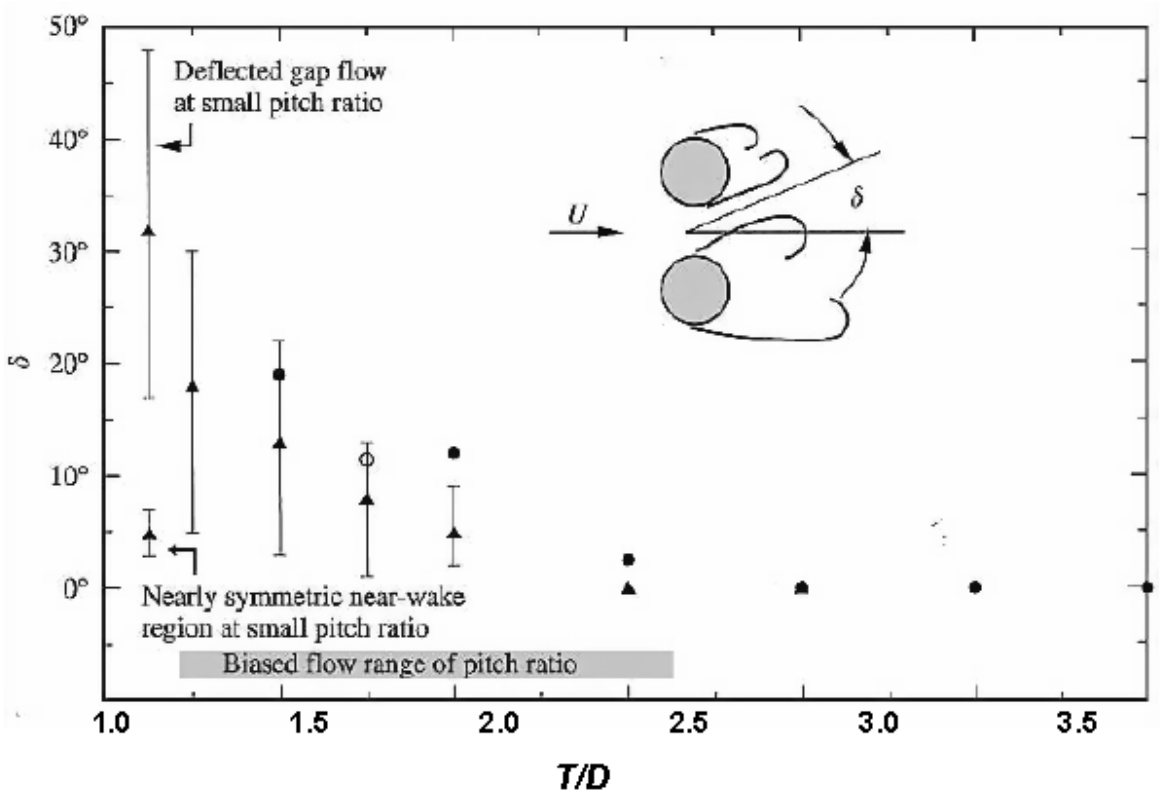

Figure 9: Graph for variation in flow deflection taken from Sumner et al (1999)

Ishigai et al. (1973) classified the flow patterns observed in inline and staggered tube bundles in five distinct regions based upon their experiment conducted for a large number of gap ratios. The flow pattern map was later modified as additional data was gathered for low gap ratios by Ishigai et al. (1977). However, for an inline square tube bundles on three of these five patterns were observed. Figure 10 was the summary of their work, which describes the various flow patterns for inline tube bundles.

For $P/D < 2$ pattern A and B were observed. For patterns C to occur, L/D should be greater than T/D.

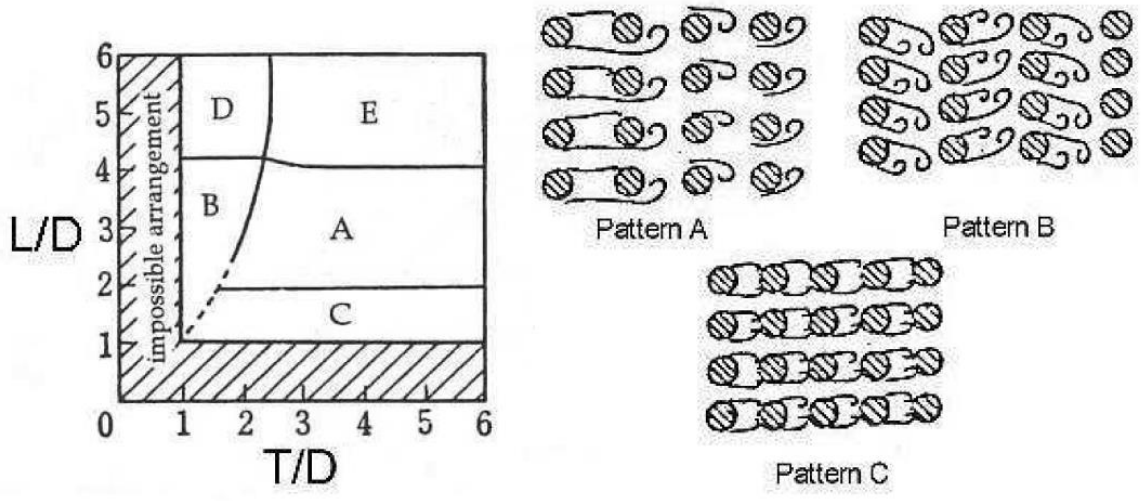

Figure 10: Flow patter classification taken from studies by Ishigai et al. (1977)

4.4 Numerical Investigations

For *P/D* = 1.4 and *P/D* = 1.6 numerical studies of Iacovides et al. (2014) showed a diagonal flow behaviour, which was in contradiction to studies by Ishigai et al. (1977) which suggests pattern A and B for *P/D* < 2. The contradiction between these two studies was due to the use of periodic boundary condition by Iacovides et al. (2014), which holds a good assumption for a large tube bundles, while the experimental studies by Ishigai et al. (1977) was done on a laboratory scale which had walls and forced the fluid to move in an non – diagonal pathway.

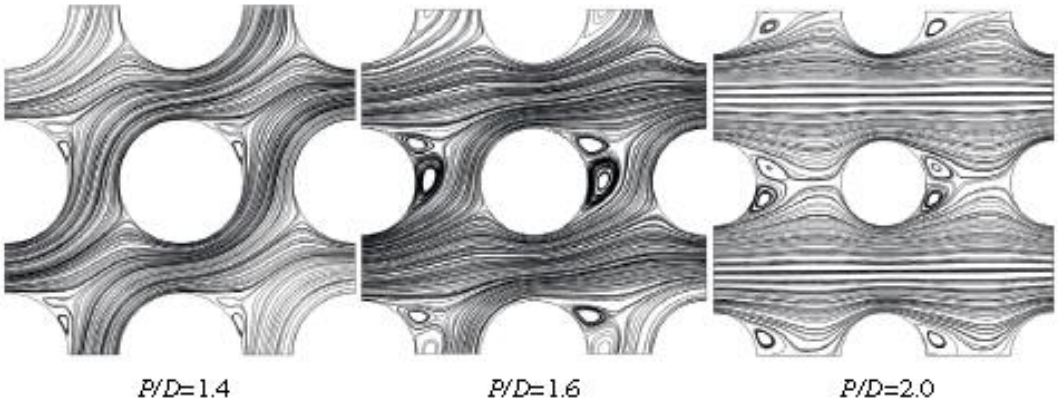

Figure 11: Flow pattern at different P/D, LES computation at Re = 41,000 by Iacovides et al., (2014)

Figure 11 shows the LES computations performed at Re = 41,000 with periodic boundary conditions of Iacovides et al. (2014) which clearly shows a diagonal flow behaviour for *P/D* = 1.4 and *P/D* = 1.6. However, an LES study performed by Afgan (2007) found no such flow behaviour at *P/D* = 1.6. The primary reason for this contradiction could be due to the use of a non-conformal block structured mesh (as non-conformal block structured meshes are known to give numerical noise), periodicity (as errors may have recycled and got amplified) and being the fact that it was close to the transition value from straight through to diagonal. For *P/D* = 2, (Iacovides et al. 2014) the flow passes from left to right without showing any diagonal deviation and also showed a higher values of time averaged turbulent kinetic energy owing the flow impinging caused by the vortex shedding on subsequent cylinders. Moreover, Iacovides et al. (2014), found the deviation of the flow to be as high as $\pm 40^0$ from the horizontal mean flow path for *P/D* = 1.4 and the vortex shedding was not observed.

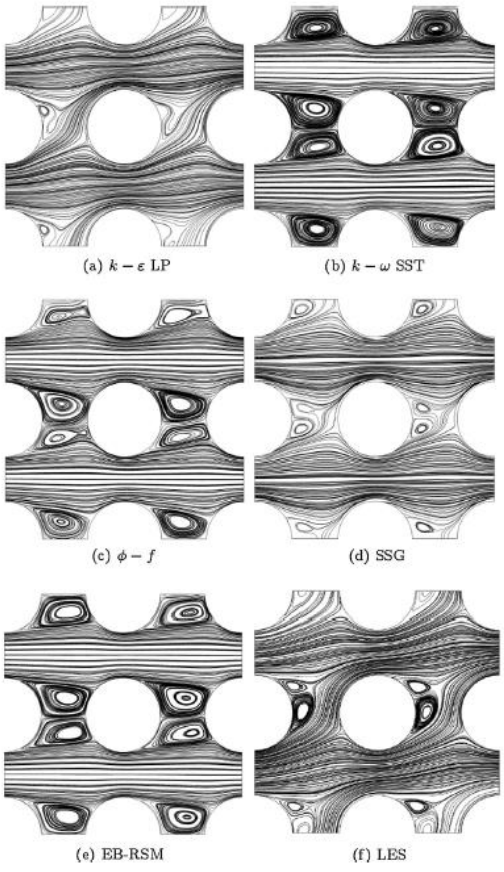

Figure 12: Flow patterns with different turbulence models (Iacovides et al. 2014)

The choice of turbulence models also has an effect on flow patterns. A comparative study done to investigate the impact of turbulence models on flow patterns was done by Iacovides et al. (2014). They modelled the flow periodically in 3D using Unsteady Reynolds Averaged Navier – Strokes equation (URANS) with three different eddy – viscosity models (EVM) and two different Reynolds Stress Transport Models (RSM) and compared with LES, in order to investigate the flow behaviour and mean flow quantities for in-line tube bundle configuration at *P/D* = 1.6 and Re = 41,000.

They stated in relation to Figure 12, *"…all the eddy-viscosity schemes exhibit a straight-through behaviour except the k–ε*

LP EVM which shows a flow pattern very similar to that of the LES results. However, this apparently satisfactory behaviour is a consequence of two serious weaknesses with this approach: the use of a wall function with seriously limited validity and a turbulence model that adopts a linear stress strain relationship. By chance, in this particular case, so far as the streamline pattern is concerned, the resulting errors have proved to be largely self-cancelling."

However, in 2D simulation (West 2013) with RSM SSG using a wall function, diagonal flow pattern was observed as seen in LES but with the same model in 3D, only a slight asymmetry in flow was observed (Iacovides et al. 2014).

Earlier studies over inline tube bundles by numerous authors conducting either computational or experimental have missed such a striking flow pattern where the flow deviates from the horizontal mean flow path. Kim (2013) chose a domain for numerical studies which takes account of symmetrical vortices formed in front and back of the cylinders and also used periodic boundary condition to model the flow suitably in two dimensions. The Reynolds numbers were 8.315×10^4 and 3.267×10^5 with $P/D = 1.4$ and $P/D = 1.6$, no asymmetric flow pattern was observed, suggesting either the eddy viscosity turbulence model used failed to capture it (as demonstrated by Iacovides et al. (2014) and West, (2013)) or such diagonal flow behaviour was not observed at these particular Reynolds numbers. Similar studies conducted by Wilson & Bassiouny (2000) saw no asymmetric flow pattern, when the flow was modelled using a eddy – viscosity model, k–ε.

The presence of a wall, suppresses the above diagonal flow behaviour observed. Iacovides et al. (2014) employed a repeating boundary condition on a 4 x 4 domain to simulate and compare the results obtained by Aiba & Hajime (1982), the results were in good agreement and no diagonal flow was observed.

4.5 Heat Transfer

The differences in flow pattern across different turbulence models have an effect on mean flow quantities as well when plotted against different location over the surface.

The models giving an asymmetric flow behaviour (as seen in the previous section) shows asymmetry in mean flow quantities as well. This was confirmed by Iacovides et al. (2014), asymmetric variation in Pressure coefficient and Nusselt number for LES and k–ε LP EVM were seen, while the other models showed symmetric variation.

Iacovides et al. (2014) further discovered, only the RSM SSG model out of the other URANS models achieved a bit agreeable result for Nusselt number (Nu) in 3D, for P/D = 1.6 when the domain has repeating boundary condition instead of periodicity. However, in 2D cases, Kim (2013) showed for Reynolds number as high as 8.315 x 10^4 and 3.267 x 10^5, the k–ω SST model performed better than the other eddy – viscosity models employed for a domain being suitably being periodic.

Reviewing extensive data on inline tube bundles, Zukauskas (1972) gave a correlation for heat transfer coefficient. In spite of its wide application, Kim (2013) pointed out its major drawback, that this correlation is only applicable when there is a variation in transverse pitch to diameter ratio. If transverse pitch to diameter ratio is kept at a constant value, the Zukauskas (1972) correlation gives a constant value as well even though the longitudinal pitch to diameter ratio is varied. To take into account the effect of variation of longitudinal pitch to diameter ratio Kim (2013) proposed a correlation by modifying the correlation of Zukauskas (1972) and also concluded that both these correlation give the same result after L/D = 2.7 as further in increase in L/D, it no longer plays any role in heat transfer.

Inferring from the work done by Kim (2013), Nu increases as L/D was increased, while keeping the T/D fixed. Moreover, Wilson & Bassiouny (2000) showed Nu increase with Reynolds number was increased for any L/D kept fixed.

4.6 Pressure

A body in the wake of another certainly has different flow physics than kept directly facing the free stream. Such is a case in tube bundles. The cylinder downstream sees the wake of another cylinder upstream and the flow physics now depends on the wake of the upstream cylinder. To address this phenomenon and thoroughly investigate a study was conducted by Traub (1990). The experimental apparatus of the mentioned

author included an open circuit wind tunnel with tube arranged in an inline and staggered fashion. The main theme of the experiment was to determine the influence of turbulence intensity and Reynolds number on pressure drop for the above mentioned configurations. A decrease in the pressure drop was seen for very high Reynolds number. The primary reason for such behaviour was due to the shrinking of the recirculation region, which happened at due to the separation point over the cylinder oscillated with the flow. However, for a very low Reynolds number flow, the recirculation region increases (Lam et al., 2003) in contrast of shrinking recirculation region for very high Reynolds number flow (Traub 1990). Lam et al. (2003) found that the increase in recirculation region shits the stagnation point which is commonly observed in front of the cylinder.

This shift in stagnation point was found to be as high as 20 – 30 degrees from the mean horizontal flow as seen from the study of Lam & Fang (1995). Such a phenomenon influences the pressure distribution around the cylinder as well. For narrow gap ratios the stagnation point shifts are even more. It goes as high as 45^0 as observed by Aiba & Hajime (1982). The primary reason for such a high shifts for low gap ratios were due to the flow asymmetry. This causes differences in pressure distributions between the top and bottom half of the cylinder.

4.7 Lift and drag coefficients

The flow pattern observed have an appreciable effect on the mean flow quantities. Periodic fluctuations have been seen as the flow oscillates. The frequency of oscillations is dependent upon the gap ratio and Reynolds number of the flow. Arie et al. (1983) investigated the effect of such oscillations on lift and drag coefficients. The cylinders were placed in a tandem arrangement. The authors reported that the lift and drag coefficients were influenced by the spacing between the cylinders and the quantities fluctuated with respect to time. These force coefficients increase with increase in spacing between the cylinders.

Fluctuations about the zero were also found by Sayers (1988) for an inline arrangement. Here, the Reynolds number of the flow was 30,000 and the spacing ratio was varied from 1.1 to 5. However, the lift coefficient fluctuated; the drag coefficient was reported the highest for spacing ratio of 1.5. The primary reason of these

oscillating coefficients about its mean is due to the flow oscillations caused by the vortex shedding. A similar behaviour of the lift coefficient was also reported by West (2013).

4.8 Strouhal Number

For vortex shedding studies, the non-dimensional parameter used for similarity studies is the Strouhal number (*St*), which is given by

$$St = \frac{fD}{U} \tag{4.1}$$

where *f* is the vortex shedding frequency, *D* is the diameter of the cylinder and *U* is the free stream velocity. Reynolds number doesn't much have an influence on Strouhal number for a fully developed flow (Sayers, 1990). An empirical relation for Strouhal number as a function of Reynolds number for a single number is given by

$$St = 0.198\left(1 - \frac{19.7}{Re}\right) \tag{4.2}$$

The above relation gives value with a good accuracy. However, the origin of the relation is not known. In-spite of being appreciably accurate for a single cylinder, it cannot be extended to tube bundles. To address this problem, Weaver et al. (1986) performed a series of experiments and produced the following relationship for inline tube bundles.

$$St = \frac{1}{2\left(\frac{P}{D} - 1\right)} \tag{4.4}$$

4.9 Conclusion

Immaterial of the Reynolds number of the flow for low gap ratios with periodic boundary condition in a numerical simulation, a diagonal flow pattern is seen. However, if URANS simulations are conducted such a flow pattern is not observed. If the flow is confined within the walls for both numerical and computational studies, diagonal flow is not observed as the wall supresses the motion. The map by Ishigai et al. (1977) is also good guide for the flow patterns observed.

For heat transfer, Nusselt number should be corrected if obtained using numerical method. The lift and drag coefficients oscillate as a result of flow oscillations caused due to vortex shedding. The pressure distribution around the surface of the cylinder is also largely depended on the flow behaviour.

Empirical relationship for Strouhal number of a single cylinder is not valid for tube bundles; hence the relationship by Weaver et al. should be used for analytical calculation of vortex shedding frequency.

Chapter 5: Numerical Treatment

5.1 Introduction

Finite Volume Methods theory is well written in couple of standard Computation Fluid dynamics text book. Ferziger and Peric (2002) have given the integral form for a general quantity, ϕ in conservational form with steady state assumption as,

$$\int_S \rho\phi v.n\mathrm{d}S = \int_S \Gamma \,\mathrm{grad}\phi.n\mathrm{d}S + \int_\Omega q_\phi \,\mathrm{d}\Omega \tag{5.1}$$

Equation 5.1, is in similar form as seen in Navier – Strokes equations, where ρ is the density of the fluid medium; S is the surface area of the control volume under consideration and Ω is the volume of the control volume under consideration. For simplicity, 2D Cartesian structured gird is considered. However, ideas presented in this section can be readily applied to unstructured grids with little modification as the face centre may or may not coincide with the intersection point of the face with the line joining the two centres of the two adjacent control volumes. Figure 13, shows a typical CV in 2D Cartesian co-ordinate system, where *N or n, S or s, E or e* and *W or w* represents north, south, east and west direction. Capital letters are used for cell centres while small letters are for face centres. This notation was followed for the entire chapter.

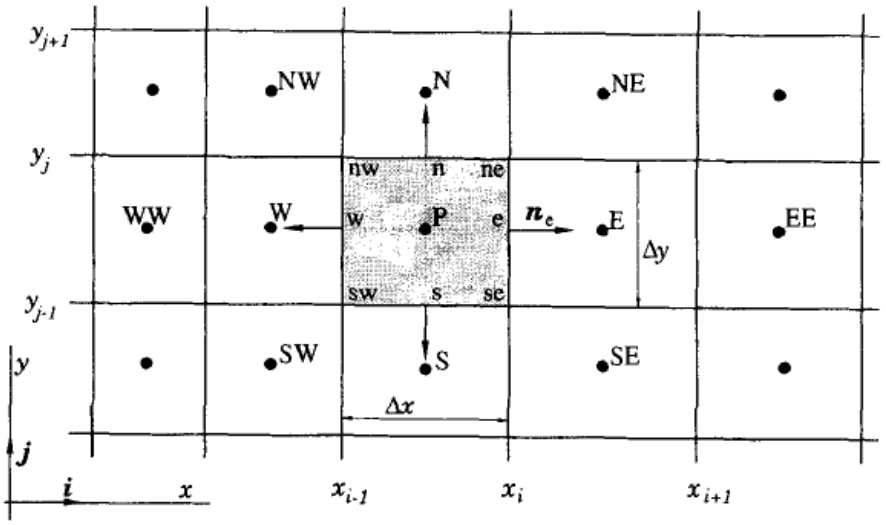

Figure 13: 2D CV in Cartesian co-ordinates taken from Ferziger and Peric (2002)

The major difference between Finite Element Method (FEM) and Finite Volume Method (FVM) are:

- In FEM, the computational points and storage are the nodes of a particular element, while, in FVM scalar properties are stored at cell centres and the velocities are stored at face centres, unless collocated grid arrangement is considered, where all the quantities are stored at cell centres.
- The governing laws in case of FEM are solved for the entire global domain and the quantities are conserved in a global sense rather local. It employs Galerkin Projection and quantities at any location in a particular cell is determined using shape functions which takes into account the nodal values of the quantity under consideration. However, the governing equations in case of FVM are solved for an individual cell and quantities are conversed for a cell under consideration rather than on a global sense.
- FEM is a popular choice for Structural related problem, while, FVM is widely used for Fluid dynamics related problems.

5.2 Approximation for Integrals

For a given CV, the net flux for an unknown quantity, ϕ is the given by the summation of all the integrals around the CV was given as (Ferziger and Peric 2002),

$$\int_S f \mathrm{d}S = \sum_k \int_{S_k} f \, \mathrm{d}S \tag{5.2}$$

where *f* is either a convective or a diffusive flux in normal direction to the face, given by $\rho\phi v.n$ or $\Gamma \mathrm{grad}\phi.n\mathrm{d}S$ respectively. Equation 5.2, serves as an approximation for surface integrals.

For volume integrals, it was written as by Ferziger & Peric (2002),

$$Q_P = \int_\Omega q\mathrm{d}\Omega = q_P \Delta\Omega \tag{5.3}$$

However, using Gauss theorem the volume integral is converted into surface integral and equation 5.2 is used.

5.3 Discretization of Navier-Stokes Equation[1]

Equation 5.2, assumes the velocity field is known. However, it is not generally known and this makes the Navier Strokes equation non – linear. The velocity also being a variable makes the problem to be solved in a coupled fashion.

The following section deals with discretization of various fluxes commonly seen in Navier Strokes Equations. The discretization stars by first integrating the momentum equation. The X – momentum equation in two dimensions is discretised as follows,

$$\iint_V \left(\frac{\partial(\rho U^2)}{\partial x} + \frac{\partial(\rho UV)}{\partial x}\right) dxdy = -\iint_V \frac{\partial P}{\partial x} dxdy + \iint_V \left(\frac{\partial}{\partial x}\left(\mu \frac{\partial U}{\partial x}\right) + \frac{\partial}{\partial y}\left(\mu \frac{\partial U}{\partial y}\right)\right) dxdy \tag{5.4}$$

Upon integration of equation for the CV as seen in Figure 13 leads to,

$$\left[\int \rho U^2 dy\right]_w^e + \left[\int \rho UV dx\right]_s^n = \left[\int \mu \frac{\partial U}{\partial x} dy\right]_w^e + \left[\int \mu \frac{\partial U}{\partial y} dx\right]_s^n - \iint_V \frac{\partial P}{\partial x} dxdy \tag{5.5}$$

5.3.1 Pressure Term

The Pressure term were approximated as follows and stored at cell centre,

$$\iint_V \frac{\partial P}{\partial x} dxdy = \left(\frac{\partial P}{\partial x}\right)_P \Delta x \Delta y \tag{5.6}$$

[1] Craft, T., 2015. Lecture notes on Computational Fluid Dynamics. The University of Manchester, UK.

Approximation applied in equation 5.6 can be used to approximate any other source term.

5.3.2 Diffusive Fluxes

The diffusive fluxes in equation 5.5 were approximated as

$$\left[\int \mu \frac{\partial U}{\partial x} dy\right]_w^e + \left[\int \mu \frac{\partial U}{\partial y} dx\right]_s^n = \left[\mu \frac{\partial U}{\partial x} \Delta y\right]_w^e + \left[\mu \frac{\partial U}{\partial y} \Delta x\right]_s^n \tag{5.7}$$

The terms $\partial U/\partial x$ and $\partial U/\partial y$ in equation 5.7 at cell faces were evaluated using central differencing scheme as follows,

$$\left(\frac{\partial U}{\partial x}\right)_e = \frac{U_E - U_P}{\Delta x}, \left(\frac{\partial U}{\partial x}\right)_w = \frac{U_P - U_W}{\Delta x}$$

$$\left(\frac{\partial U}{\partial y}\right)_n = \frac{U_N - U_P}{\Delta y}, \left(\frac{\partial U}{\partial y}\right)_s = \frac{U_P - U_S}{\Delta y} \tag{5.8}$$

5.3.3 Convective Fluxes

The convective fluxes were discretised as follows,

$$\left[\int \rho U^2 dy\right]_w^e + \left[\int \rho UV dx\right]_s^n = [\rho U^2 \Delta y]_w^e + [\rho UV \Delta x]_s^n \tag{5.9}$$

this can be further written as follows,

$$[\rho U^2 \Delta y]_w^e + [\rho UV \Delta x]_s^n = (\rho U \Delta y)_e U_e - (\rho U \Delta y)_w U_w + (\rho V \Delta x)_n U_n - (\rho V \Delta x)_s U_s \tag{5.10}$$

In contrast to the diffusive fluxes the convective fluxes discretisation contains the quantities to be evaluated at the face centres instead of cell centres. In a collocated

storage arrangement, the values were stored at the cell centres. Suitable approximations were needed to evaluate the value at face centres from cell centre values.

There are three widely used approximation used, namely,

- Upwind scheme – First or second order accurate.
- Central Difference Scheme – Second order accurate.
- QUICK scheme – Third order accurate.

In the simulations performed for tube bundles second order treatment was given to discretise all the spatial variables. Hence, only the Central Difference Scheme is presented in the sub sequent section.

5.3.3.1 Central Difference Scheme

To obtain the quantities at face centres, Taylor series expansions were performed at the two adjacent cell centres along a particular direction. The resulting approximation for velocity at each face are given as follows,

$$U_e = 0.5(U_E + U_P),\ U_w = 0.5(U_P + U_W)$$
$$U_n = 0.5(U_N + U_P), U_s = 0.5(U_P + U_S) \tag{5.11}$$

Note that Equation 5.11 gives second order approximation for the convective fluxes, and being a second order scheme it gives oscillations in the solution. This problem was solved using Semi Implicit Method for Pressure Linked Equations (SIMPLE) scheme of Patankar and Spalding (1972).

5.3.4 Pressure – Velocity coupling

For the range of Reynolds number (250 – 1,000), the Mach number (*M*) was found to be less than 0.3, making the incompressible flow assumption valid. In an incompressible flow the absolute pressure was immaterial, only the pressure gradient was needed. The pressure was then obtained by solving the Poisson's equation.

It also became mandatory to obtain a forth equation, as the pressure was not explicitly present in the continuity equation. The SIMPLE scheme of Patankar and Spalding (1972) was used for pressure and velocity corrections.

5.3.5 Time Discretization

Due to vortex shedding observed in tube bundles making the problem under consideration inherently unsteady, an Euler implicit first order time scheme was used to march in time. The above numerical scheme was still applicable with an additional term (time) in the Navier – Strokes equation.

The first order Euler Implicit time scheme can be written in a concise form as,

$$\phi_i^{n+1} = \phi_i^n + F^{n+1}\Delta t \tag{5.12}$$

where, n denotes the time level, i denotes the spatial location, F is the convective/diffusive fluxes and Δt is the time step. The non-dimensional time step was considered and kept at a constant value of 0.05 for all the simulations performed.

The major advantage of an implicit scheme over an explicit scheme, it is inherently stable. However, for accuracy if the solution is time dependent, large time steps will result in large errors.

5. 4 Boundary Conditions

In engineering problems a boundary is a necessary requirement, which defines the limit of the system under consideration. In numerical simulations, there are two ways to specify the conditions over a boundary, namely, Neumann and Dirichlet.

Dirichlet boundary condition specifies the value of some variable over the boundary, for example, temperature. While, Neumann boundary condition specifies the gradient normal to the surface for some variable, for example, heat flux.

While setting up the simulation, at the cylinder walls, Neumann boundary condition is prescribed setting the mass flux and pressure to be zero. The Energy equation was not

solved as the main aim of this work was to study the flow physics and conduct uncertainty quantification for lift & drag coefficient and also the skin friction coefficient. Hence, it was not required to specify any boundary condition for thermal parameters over wall or anywhere in the domain.

Periodic boundaries are treated as internal surfaces and not boundaries. Hence, a specification was not necessary. However, mass flux and pressure drop were suitably prescribed.

5. 5 Conclusion

This chapter has briefly described the numerical treatment provided to each individual term in the Navier – Strokes equation and dealt with relevant aspects of Finite Volume Method's theory used for numerical solution of flow.

Chapter 6: Turbulence

6.1 Introduction

A wide range of engineering problems are inherently turbulent in nature. Hence, it becomes necessary to deal with approximations and assumptions for modelling turbulent flows. Turbulence consists of random or chaotic motion for the fluid. Eddies of all sizes and shapes are observed in a turbulent flow. The largest eddy dissipates its turbulent energy to the smaller ones and subsequently the smallest eddy dissipates its energy to heat. These eddies enhance mixing, which is quite beneficial in an engine to enhance fuel and air mixing.

In tube bundles turbulent mixing further enhances heat transfer rates and are important flow structures is also vortex shedding observed in it. Modelling them becomes a challenge owing to the chaotic nature. Research is still ongoing which is primarily motivated due to its wide applicability in engineering problems.

The classic parameter to classify the flow regimes, namely, laminar, transition or turbulent is the Reynolds number (*Re*). It is named in the honour of Osbourne Reynolds who conducted a pipe flow experiment in Manchester in order to study Fluid Dynamics in greater detail.

This chapter deals with some aspects of turbulence and its modelling in brief.

6.2 Origin of Turbulence

Chaotic movement of a fluid is often termed as turbulence. There is no one way of turbulence generating in a flow. Turbulent flows are flows which are unstable in nature. A laminar flow can show instability due to three different effects,

- Fluctuations rising due irregular surfaces (Conde & Vassilicos, 2000).
- Fluctuations due to complex motion.
- Due to body forces.

In regards to fully developed turbulent flow, Hunt el al. (2005) have stated, *"A fully developed turbulence is reached when one or more of these processes has generated velocity fields that are chaotic in space and time, having smooth spectra and smooth probability distributions. Once this state is reached, which requires that the Reynolds number is large enough, these general qualitative properties are observed not to change even when quite substantial perturbations are introduced…"*

Recent research is focused on determining the different aspects leading to unstable fluctuations form laminar to fully turbulent flows. Initial there were two propositions (Williams et al., 1969). The first one dealt with slow transition from laminar to turbulent flows. It considered a slow transition; occurred when the shear layer was initially unstable only in a single mode, and later on it develop other distinct modes due to non-linear interactions, e.g., wakes. The second one was a fast transition, occurred when the scales of velocity fluctuations develop rapidly and where turbulent scales where comparable to that of a fully developed turbulent flow, e.g., pipe flows.

It cannot be guaranteed turbulence will be seen for a particular Reynolds number, it is more dependent on the extent of the boundary layer in streamwise direction. Huerre & Monkewitz (1990) termed as 'convective' for instabilities commonly seen in slow transition which might or not lead to turbulent flows. However, in fast transition the absolute instabilities form the most part of the domain. The transition here is generally rapid, irrespective of convective or absolute instabilities.

6.3 Eddy

The quantification of eddies reply on statistical methods. Broadly classified in to three types based on the type of eddy and sampling methods employed (Bonnet & Glauser, 1993). The first type determines the modes in a particular co-ordinate system using two point Eulerian correlations (Devenport, 1999). The second one used the data obtained at high Reynolds number. This velocity data, normally obtained by numerical simulation as they give complete velocity field in the given domain, was used to determine the structure of an eddy (Arneodo et al., 1999). The third one used

the combination of the above two (Tabeling, 1999), it required, eddies to be close to each other.

Viscosity leads to dissipate the turbulent energy of the smallest eddies dissipate into heat. From dimensional analysis the smallest eddies relates to kinematic viscosity (v) as[2],

$$(v^3/\varepsilon)^{1/4} \tag{6.1}$$

From equation 6.1, it can be seen as the kinematic viscosity reduces the size of the smallest eddies also reduces and for the definition of Reynolds number, as it increases the kinematic viscosity decreases.

6.4 Turbulence Modelling

There are several approaches to model turbulence and it was classified in six different categories by Bardina et al. (1980), as,

- Direct Numerical Simulation (DNS)
- Large Eddy Simulations (LES)
- Two Point closure
- One point closer
- Integral Equations
- Correlations

In the present simulation one point closer was used to model the flow. It used a two equation linear Eddy Viscosity model, known as $k - \varepsilon$ by Launder and Spalding (1974) which is dealt in the next section.

6.5 $k - \varepsilon$ (Linear Eddy Viscosity Model)

The $k - \varepsilon$ turbulence model by Launder and Spalding (1974) is widely used in the industry due to its simplicity and comparatively low computational cost as compared to other methods listed above. However, it has major drawbacks considering the

[2] Launder, B. E., (2016). Lecture on Turbulence. The University of Manchester, UK.

assumption used to formulate the model. The assumption involved can be listed down as,

- The flow is considered to be simple shear.
- The generation of turbulent kinetic energy (P_k) is equal to the dissipation rate, ε (assuming local equilibrium)
- The turbulence is unaffected by any other force.

Local equilibrium assumption would only give $\overline{uv}$ stress which was consistent with simple shear flow assumption. This idea was further adapted to give all the shear stress by considering the flow to be a simple shear flow in all directions.

Despite of several drawbacks reported by several authors, Wilson and Bassiouny (2000) produced quite satisfactory results using this model for inline and staggered arrangement of tube bundles.

In the present numerical simulation using this model, all model constants were kept default and the simulation was performed using Star CCM +.

6.6 Conclusion

The simple shear flow assumption extended in all directions aids in modelling all turbulent shear stresses. However, considering the flow in a local equilibrium have serious consequences in certain scenarios, such as a flow impingement or in an adverse pressure gradient. For such cases a suitable turbulence model should be employed.

Chapter 7: Computational setup

This chapter deals with aspects required for numerical simulation.

7.1 Domain

Iacovides et al. (2014) investigated the size of the domain required to capture the flow physics in inline tube bundles. It was concluded by the authors a grid of 2 x 2 tubes was sufficient. Afgan (2007) reported the same and further added; along the third direction, a length of two tube diameters was sufficient to capture the vortices and its effects.

In this numerical case for inline tube bundles a domain of 2 x 2 was chosen and the flow was treated to be varying in only two spatial dimensions. Block structured mesh strategy was employed. The blocks were divided in to a central core region and around the wall boundaries. Figure 14, shows the block structure of 2 x 2 domain for P/D = 1.6.

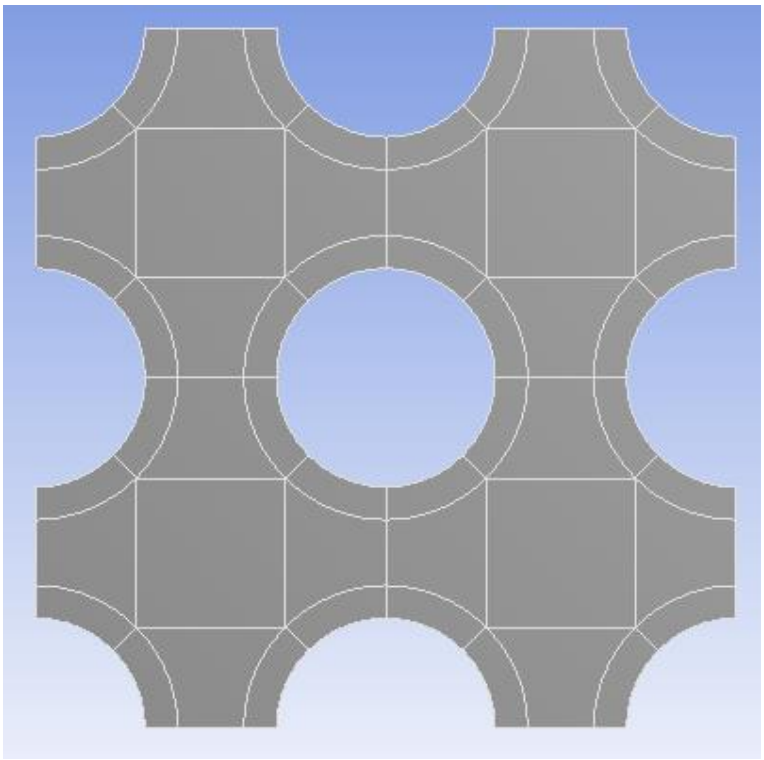

Figure 14: Blocks for 2 x 2 inline tube bundles grid for *P/D* = 1.6

7.2 Low Re grid refinement

A low Re grid resolves the viscous sublayer instead of only relying on a wall function. Resolution of boundary layer implies that the quantities determined near the required boundary generally would give better approximation. However, if the quantities rely on the flow structures within the domain, a wall function along with a High Re grid would also return good approximation.

The grid was initially had 50 cells in the central square section and 30 cells normal to the cylinder boundaries. Using this grid a simulation was carried out for inline tube bundles with P/D =1.6 and Re = 500 in order to determine the y^+ values around the cylinder walls. For a low Re grid the necessary condition was to maintain the y^+ values less than one. The grid around the cylinder walls was refined until this condition was met, while keeping the number of cells in the central region a constant. The second Grid constructed had 60 cells normal to the cylinders.

Table 4, summaries the number of cells used in different blocks for each individual grid.

Grid	Cells near cylinder walls	Cells in central square region
1	30	50
2	60	50

Table 4: Summary of cells in the domain for Low Re grid

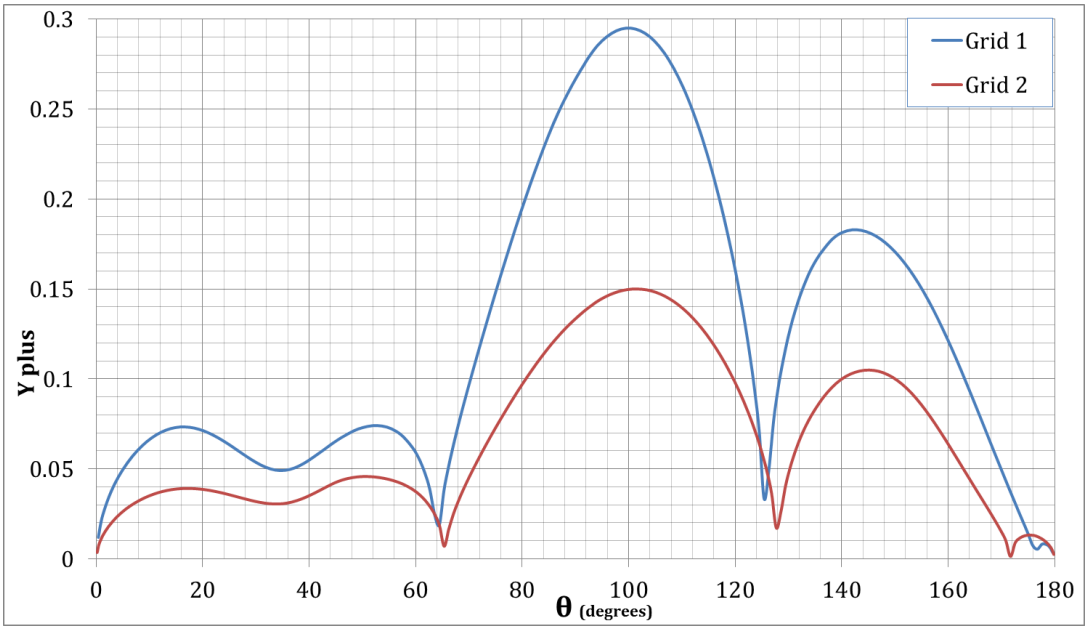

Figure 15: y^+ values for different grids around the central cylinder

Figure 15, shows the plot of y^+ values along the central cylinder. It was seen that the necessary condition was achieved in the first grid itself. Hence, along the cylinder for resolving the viscous sublayer the same grid refinement used in grid 1 was used for all simulations conducted here after. The angle notation used was as per Figure 16. The same notation was followed in writing of this chapter.

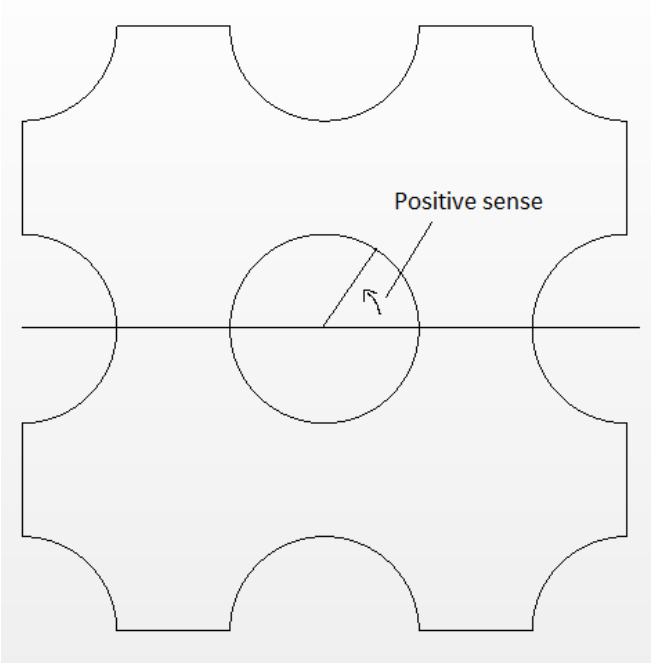

Figure 16: Angle notation around the cylinder

7.3 Mesh Independent study

Once 30 cells normal to the cylinder was established giving $y^+ < 1$. The central square block was refined until the numerical solution was grid independent. For determining the grid independency a case with $P/D = 1.6$ and $Re = 500$ was solved for different grid refinement levels. As summarized in Table 5. The pressure coefficient around the central cylinder was used to determine the mesh independency.

Grid	Cells near cylinder walls	Cells in central square region
1	30	50
2	30	100
3	30	150
4	30	250
5	30	300
6	30	350
7	30	400

Table 5: Summary of cells for mesh independent study

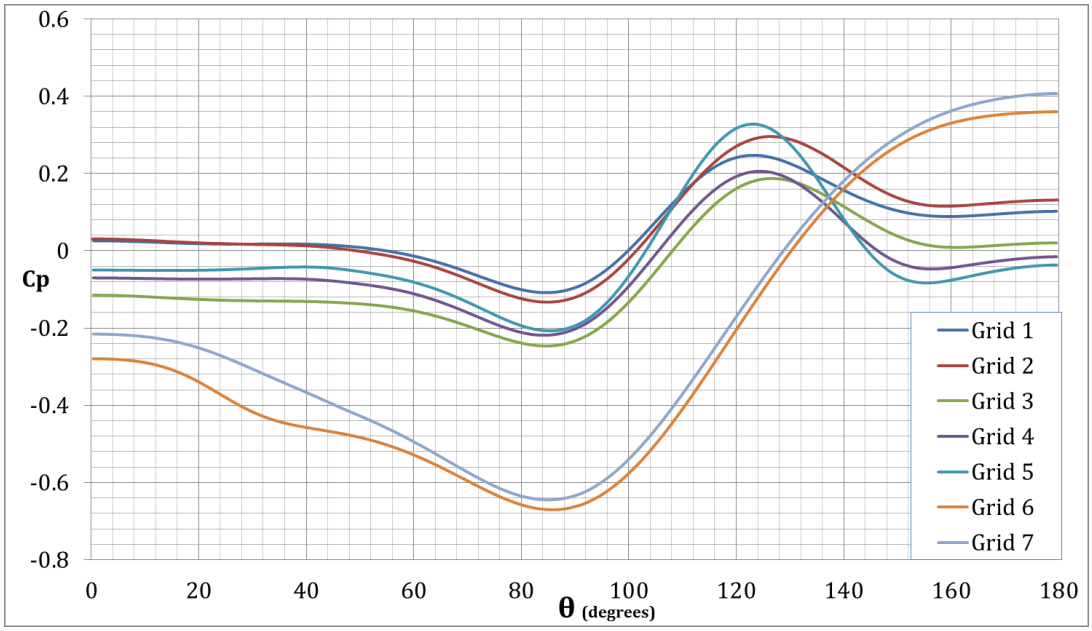

Figure 17: Pressure coefficient plot around the central cylinder for mesh independent study

From Figure 17, it was seen that the Pressure coefficient values for Grid 6 and Grid 7 around the cylinder was nearly the same. Hence, the refinement level of Grid 6 was

used for all the simulations conducted here after. Figure 18 shows the final mesh with refinement level of Grid 6.

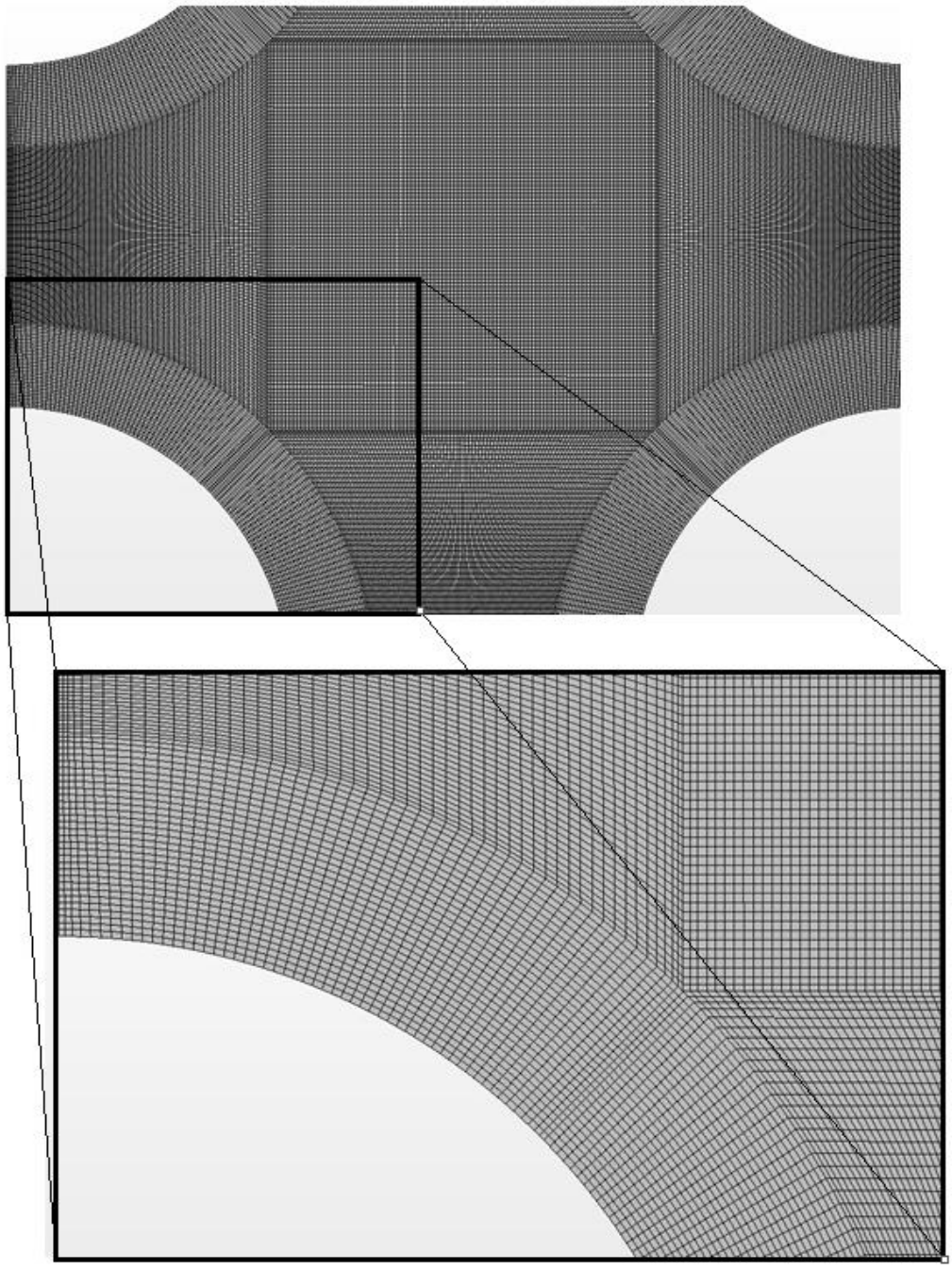

Figure 18: Finalized mesh refinement level

7.4 High Performance Computing (HPC)

Numerical simulation was too computationally intensive as it was an unsteady problem. Hence, to speed up the simulation the HPC cluster at the University of

Manchester was used. Using multiple cores doesn't always speeds up the simulation; it could sometimes increase the total computational time. To determine the number of core required for this purpose, benchmark script[3] for Star CCM+ was used for *P/D* = 1.6 & *Re* = 500 before solving all the other cases.

The following output was generated by the benchmark script,

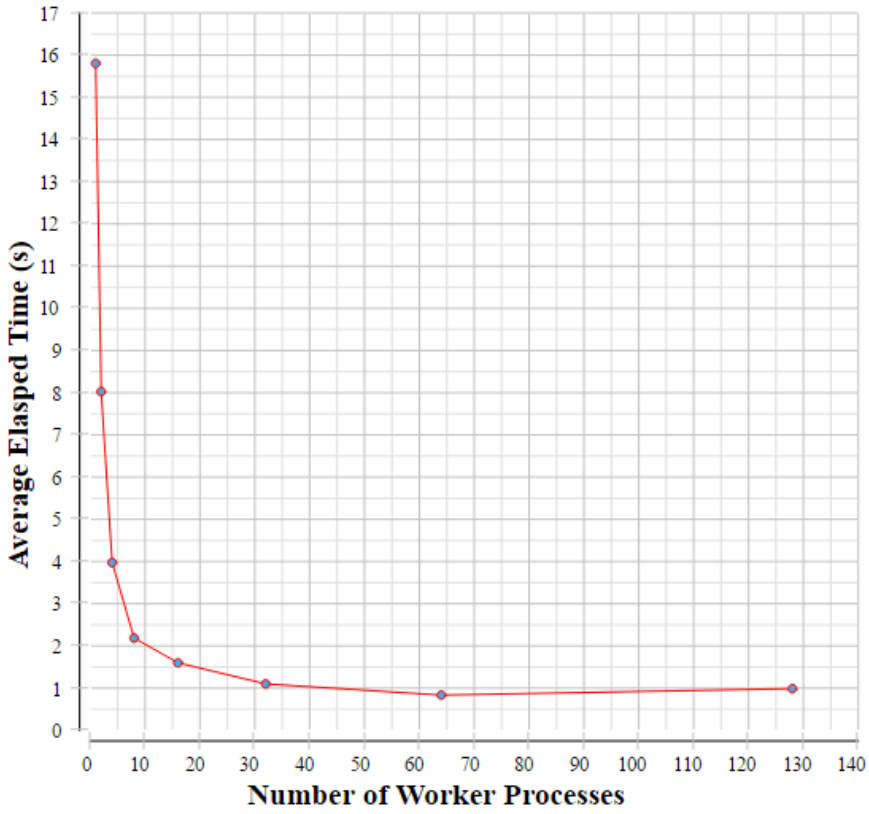

Figure 19: Computation time v/s number of processors on HPC

[3] The benchmark script file was given on the University of Manchester's (UK) website. http://ri.itservices.manchester.ac.uk/csf-apps/software/applications/starccm/

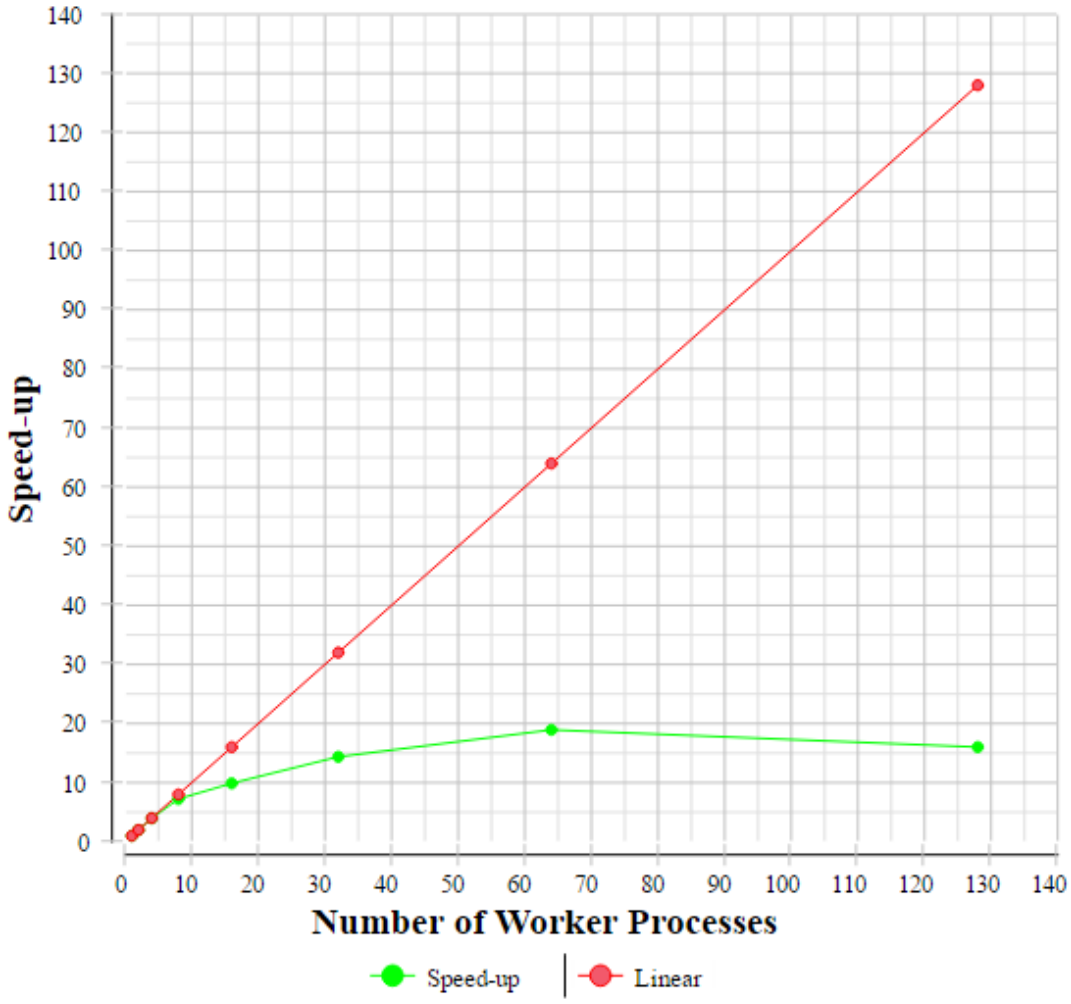

Figure 20: Speed up v/s no. of processor used in HPC

From Figure 19, it was seen that there was no substantial change in computational time between 32 and 64 cores and only it speeded up by a small percentage for 64 cores when compared to 32 cores (Figure 20). Hence, for all simulations conducted here after 32 cores were used on HPC cluster.

Chapter 8: Results and Discussion

8.1 Introduction

The main theme while writing this chapter was uncertainty quantification of square inline tube bundles. The last part of this chapter verifies the results obtained by gPC; by comparing it to the CFD result.

8.2 Uncertainty Quantification

Reynolds number of the flow and *P/D* for a square inline tube bundle was considered to be uncertain. The random variable used in the Hilbert space were ξ_1 and ξ_2 respectively. The range in the real space were considered as follows,

$$250 \leq Re \leq 1000, \quad 1.5 \leq P/D \leq 5 \tag{8.1}$$

In the Hilbert space, $-1 \leq \xi_1, \xi_2 \leq 1$ as Legendre polynomials were used for uncertainty quantification using gPC. Transformations were carried out to map the variables in the Hilbert and real space, similar to what was done in chapter 3.

8.2.1 Pre – processing

Six Quadrature points were considered in each of the random dimension as it was seen in chapter 3; it provided results of sufficient accuracy. The gPC pre – processor provided the six Quadrature points for both Reynolds number and *P/D* as listed in

Table 6.

36 numerical simulations of tube bundle were carried out by considering a Quadrature point of Reynolds number and *P/D* at a time. The coefficients of Lift, Drag and Skin friction were determined for each case. The values of each coefficient were fed into the gPC post – processor to obtain the values for the entire range of Reynolds number and *P/D*.

Serial No.	Quadrature Point for Reynolds number	Quadrature Point for *P/D*
1	275.32	1.6181
2	377.046	2.09288
3	535.51	2.8324
4	714.482	3.6675
5	872.95	4.4071
6	974.67	4.8818

Table 6: Quadrature points for inline tube bundles

The post - processing of tube bundle numerical simulation, showed that the lift coefficient oscillated as the time progressed. A result consistent with square inline tube bundle results of Iacovides et al. (2014) for *Re* = 41,000. Hence, the mean value of the solution was used for uncertainty quantification. Interestingly enough the lift coefficient fluctuated about the zero value, the same result was also reported by Sayers (1988). Figure 21, shows the lift coefficient's oscillation for *P/D* = 1.6181 and different Reynolds number with non – dimensional time step Δt^{+}, given as,

$$\Delta t^{+} = \frac{\Delta t U_g}{D} \tag{8.2}$$

where, U_g is the gap velocity and *D* is the tube diameter.

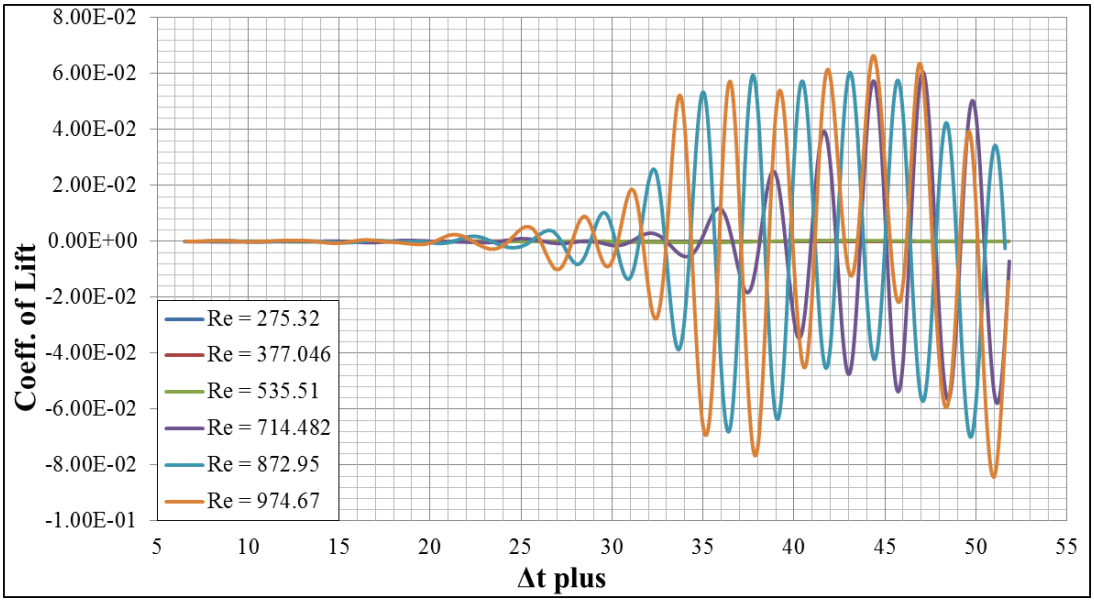

Figure 21: Fluctuations in lift coefficient with respect to time for *P/D* = 1.6181

From Figure 21, it can be seen that for different Reynolds number the amplitude of the oscillation was different. As all 36 cases were unsteady in nature the mean values of the other coefficients, namely, drag and skin friction were considered for uncertainty quantification.

The mean values for the lift, drag and skin friction were as per tabulated in Table 7,

Table 8,

Table 9.

C_L						
P/D	*Re* = 275.32	*Re* = 377.046	*Re* = 535.51	*Re* = 714.482	*Re* = 872.95	*Re* = 974.67
1.6181	-4.21E-06	-7.08E-06	2.52E-05	-4.76E-04	-4.73E-04	-2.35E-04
2.09288	-4.26E-06	1.74E-04	1.05E-03	-1.02E-02	-2.07E-03	-1.03E-02
2.8324	-5.64E-04	0.016890762	-0.015100579	0.007554542	-0.008487915	0.030292177
3.6675	1.31E-03	0.018964806	-0.014365938	-0.018094786	0.022438763	0.012684991
4.4071	-1.52E-03	-7.89E-03	-0.004224772	-0.003604092	0.00406426	0.000387001
4.8818	-0.004214878	0.007072908	0.006724049	0.009189294	-0.002459967	0.001269452

Table 7: Mean lift coefficient

C_D						
P/D	*Re* = 275.32	*Re* = 377.046	*Re* = 535.51	*Re* = 714.482	*Re* = 872.95	*Re* = 974.67
1.6181	8.54E-02	6.57E-02	4.76E-02	3.89E-02	3.47E-02	3.24E-02
2.09288	5.33E-02	4.04E-02	2.99E-02	7.63E-02	7.39E-02	7.22E-02
2.8324	1.00E-01	0.152150113	0.15423499	0.162941797	0.109987677	0.143095347
3.6675	1.54E-01	0.145090297	1.30E-01	0.168126223	0.1789864	0.18354511
4.4071	8.88E-02	1.01E-01	0.123813315	0.11336783	0.122041113	0.250845404
4.8818	0.207119088	0.220770368	0.242672736	0.263764221	0.2547623	0.250845404

Table 8: Mean Drag coefficients

C_f						
P/D	*Re* = 275.32	*Re* = 377.046	*Re* = 535.51	*Re* = 714.482	*Re* = 872.95	*Re* = 974.67
1.6181	2.70E-02	2.10E-02	1.51E-02	1.27E-02	1.19E-02	1.13E-02
2.09288	2.14E-02	1.68E-02	1.29E-02	2.39E-02	2.31E-02	2.24E-02
2.8324	3.44E-02	0.045651511	0.042705512	0.039505708	0.031829529	0.030390821
3.6675	5.22E-02	0.045900095	0.040013333	0.039721918	0.03793833	0.031856155
4.4071	3.50E-02	3.49E-02	0.034870145	0.031099202	0.027009791	0.038800294
4.8818	0.065887866	0.01472296	0.056605435	0.046344543	0.041014468	0.038800294

Table 9: Mean skin friction coefficient

8.2.2 Post – processing

The gPC post processor gave the following output for lift, drag and skin friction coefficient.

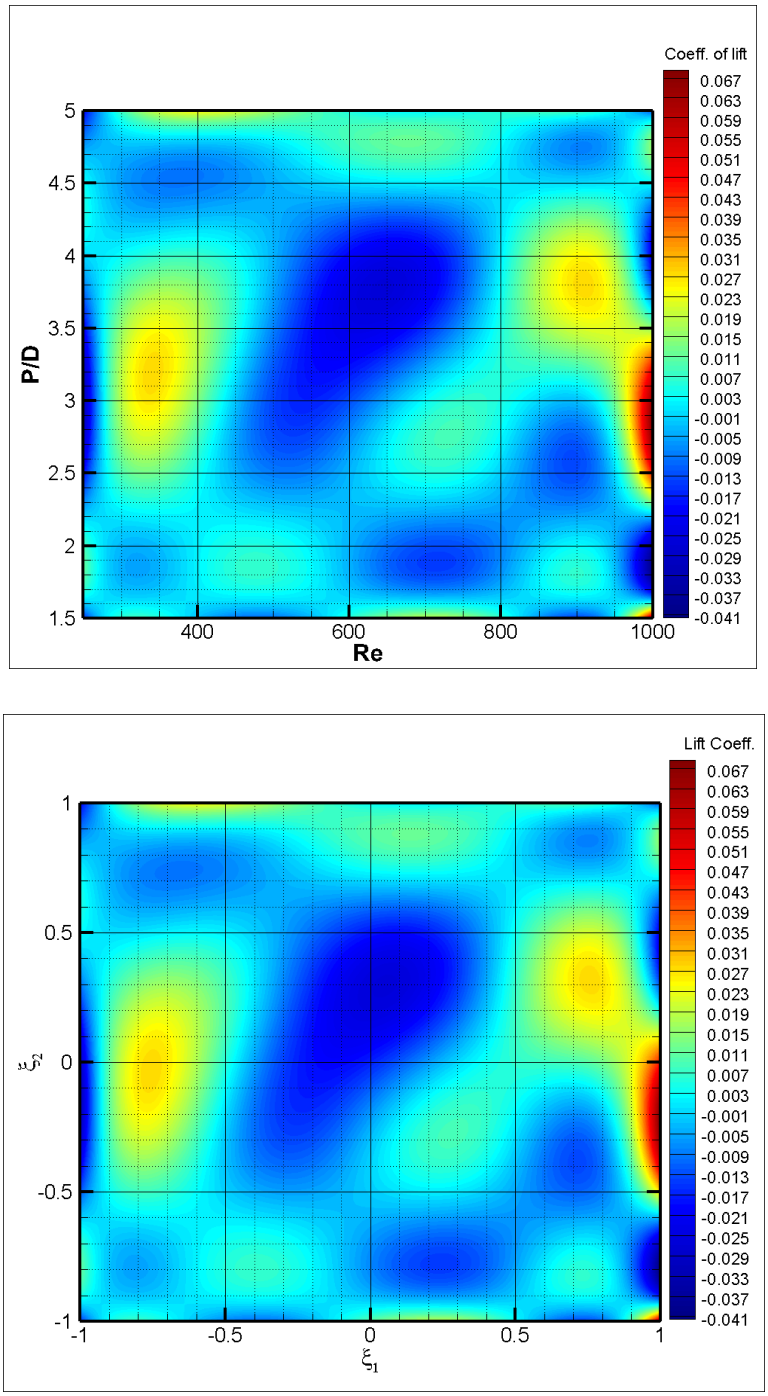

Figure 22: gPC result for lift coefficient in real space (above) and Hilbert space (below)

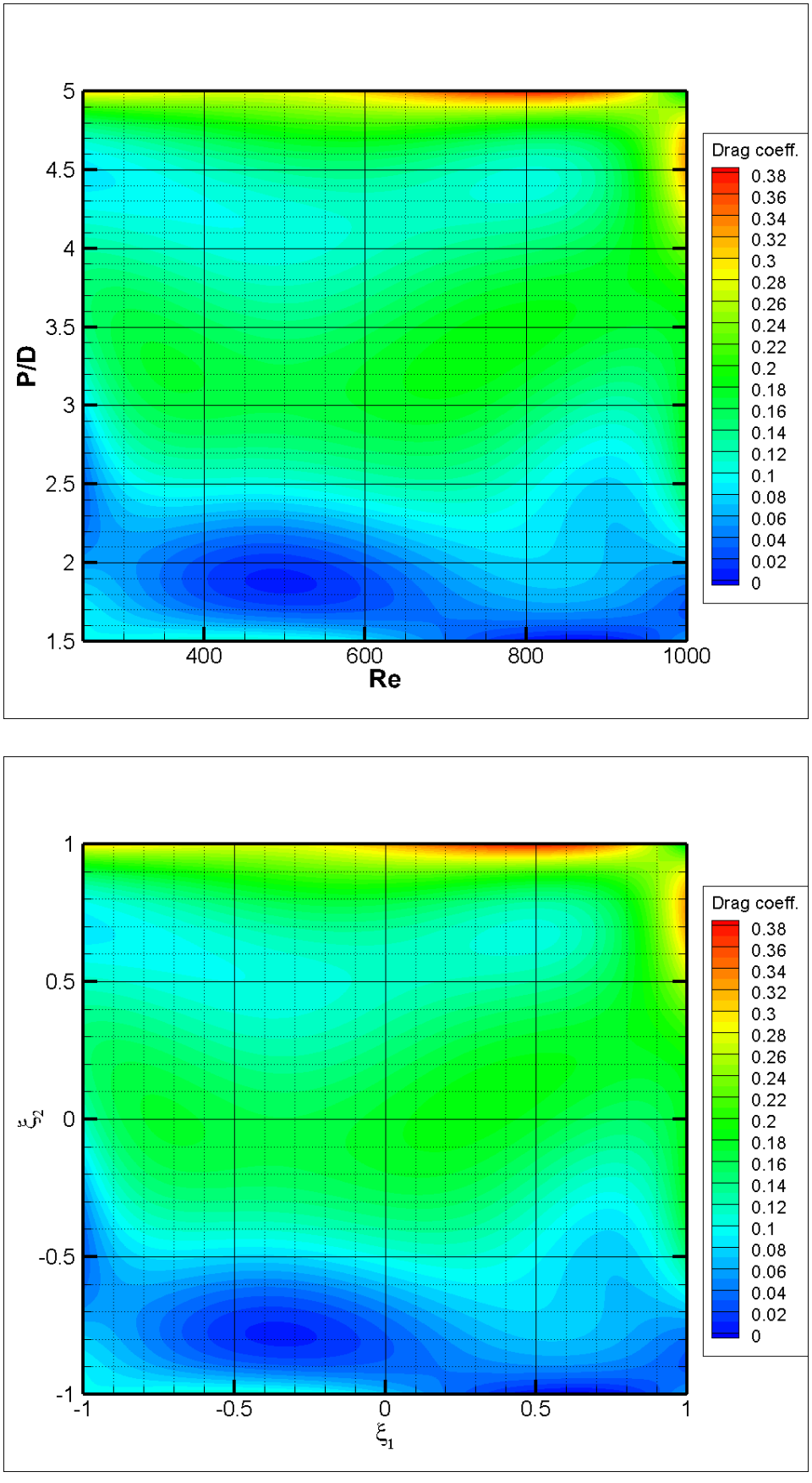

Figure 23: gPC result for Drag coefficient in real space (above) and Hilbert space (below)

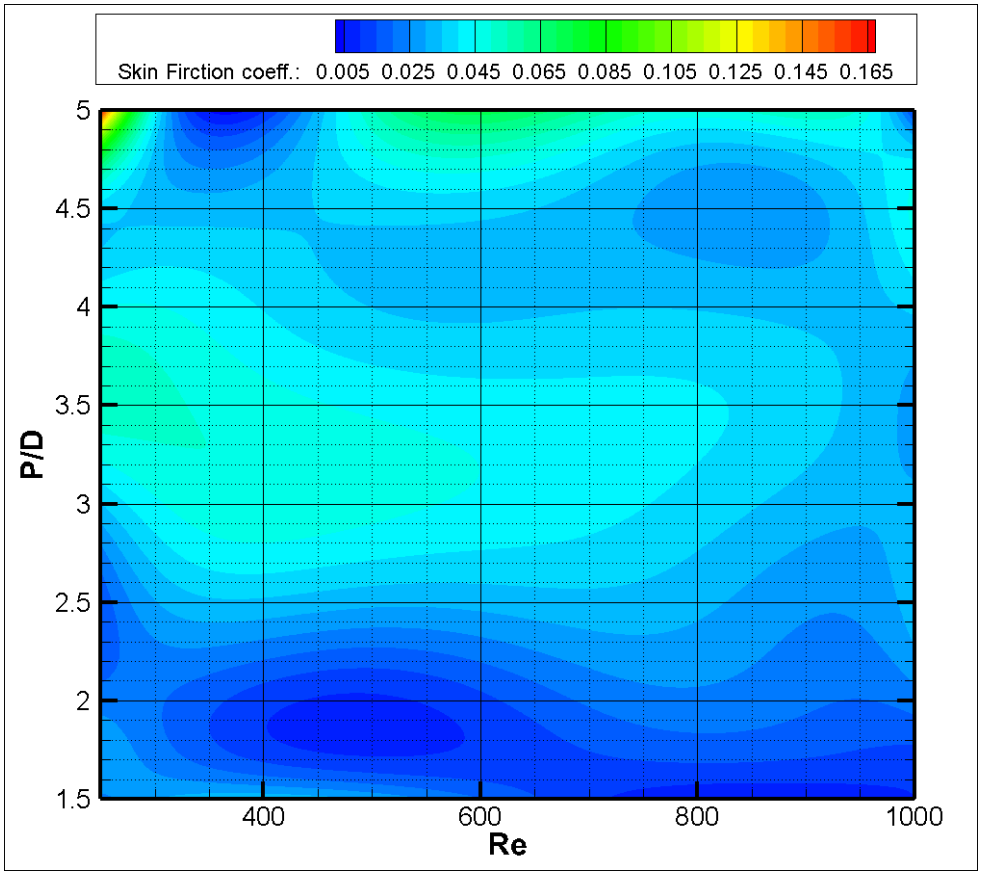

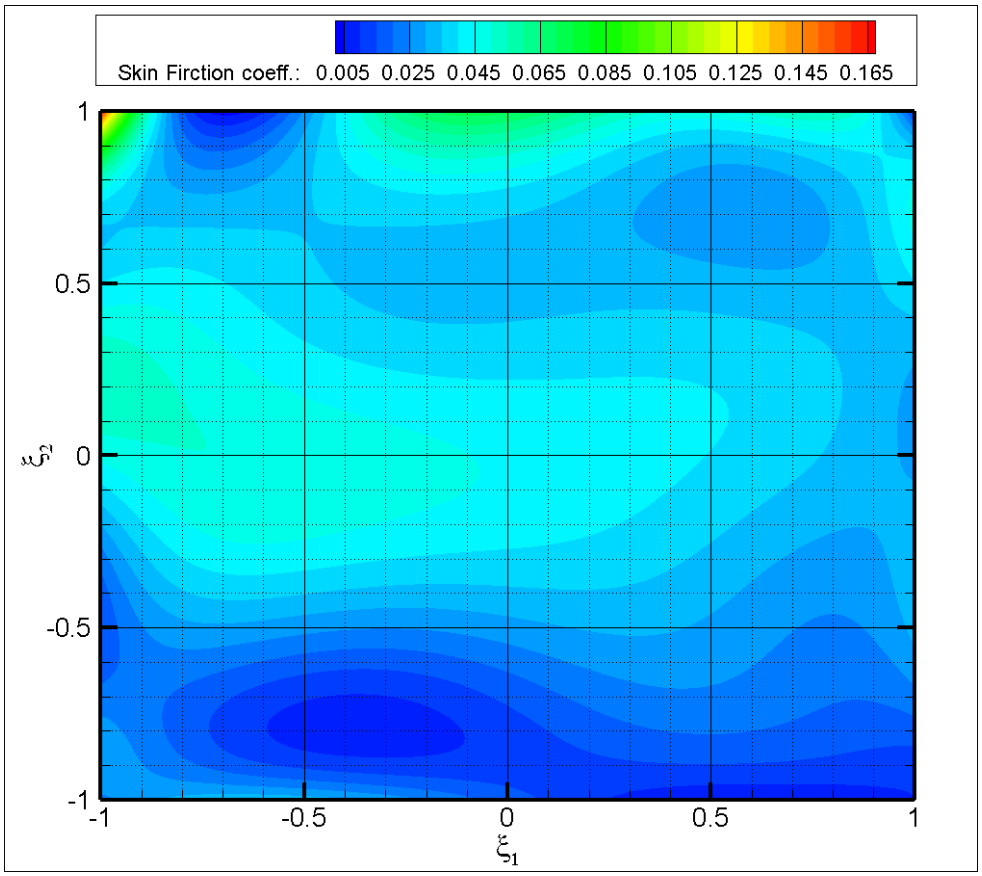

Figure 24: gPC result for skin friction coefficient in real space (above) and Hilbert space (below)

Figure 22, Figure 23 and Figure 24 were the results by gPC postprocessor in real and Hilbert space for lift, drag and skin friction coefficient respectively.

8.2.3 Verification

For the purpose of verification of the gPC result, a simulation was performed at *P/D* = 1.6 and *Re* = 500. The values obtained by simulation were,

Result	C_L	C_D	C_f
CFD	2.52E-05	5.40E-02	1.72E-02
gPC	0.002	0.05	0.0275

Table 10: Mean values for *P/D* = 1.6 and *Re* = 500

Referring from Table 10, the CFD results and the gPC result for coefficient of drag were agreed with each other. Also the skin friction coefficient was also quite close to each other. While the gPC result for lift coefficient were very different from the CFD result. However, the failure in results wasn't due to gPC. It happened due to plotting the contours of gPC results. As making the contour plots involves grouping & averaging of many discrete values and providing a single value for a region.

From Figure 22, it can be seen the value of coefficient of lift was between -0.001 to 0.003, and the CFD result lies between this range, making the gPC result valid. For the purpose of representation on paper, legend of these plots had to be of a suitable size, thus limiting the values represented by it. Errors in the contour plots could be avoided by increasing the number of values represented by its legend.

8.3 Conclusion

Uncertainty quantification using non – intrusive gPC, accurately determines the results for a given range. However, representation of this raw data could lead to errors. Hence, care should be taken while representation.

Chapter 9: Conclusions & Recommendations

gPC results for either univariate or multi – variate case gave good approximations of the solution. However, care should be taken while representing such data because it may lead to errors in the final solution. The overall accuracy of the gPC data was also dependent on the number of choice of Quadrature Points. While selecting the number of Quadrature Points the following points should be taken into consideration,

- There should be at least one Quadrature point near or at the minima or maxima of a function.
- There should be at least one Quadrature point immediate before and after the point where the gradient changes its sign.

If the function or the variation of a certain property is unknown, then running the same experiment with gradual increase of the number of Quadrature points and making suitable comparisons should be a good practise before coming to any conclusion. However, in the present study the choice of six Quadrature points gave solution of reasonable accuracy.

It wasn't mandatory to use the same order of polynomial as the number of Quadrature points. In fact, the number of Quadrature points could be higher than the polynomial order, but it may not give the best approximations. For the same order as the number of Quadrature points, it was well known fact it gives better results than fore mentioned case.

Any orthogonal polynomial from the Askey scheme could be used for gPC. If the mapping between the real and Hilbert space becomes cumbersome, then selection of polynomial should be such that the two spaces coincide with each other.

It is to be noted that the total number of computational points required rises with the power of the total number of dimensions, which is also referred to as the '*curse of dimensionality'*.

The present study was focused on modelling the coefficients of lift, drag and skin friction. However, it could be readily applied to any dependent quantity for an independent uncertain quantity.

This could be also applied in determining the flow field or turbulent fluctuating quantities, which in experimentation is only taken at certain key locations while the entire flow field still remains unknown.

Bibliography

Aiba, S. and Hajime, T. (1982). Heat Transfer Around Tubes in Inline Tube Banks. *Bulletin of the JSME*, 25(204), pp.919 – 924.

Afgan, I. (2007). Large Eddy Simulation of Flow Over Cylindrical Bodies Using Unstructured Finite Volume.

Arie, M., Kiya, M., Moriya, M. and Mori, H. (1983) 'Pressure fluctuations on the surface of Two circular cylinders in tandem arrangement', *Journal of Fluids Engineering*, 105(2), p. 161. doi: 10.1115/1.3240956.

Arneodo, A., Manneville, S., Muzy, J.F. and Roux, S.G. (1999) 'Revealing a lognormal cascading process in turbulent velocity statistics with wavelet analysis', *Philosophical Transactions of the Royal Society A: Mathematical, Physical and Engineering Sciences*, 357(1760), pp. 2415–2438. doi: 10.1098/rsta.1999.0440.

Askey, R. and Wilson, J. (1985) 'Some basic hypergeometric orthogonal polynomials that generalize Jacobi polynomials', *Memoirs of the American Mathematical Society*, 54(319), pp. 0–0. doi: 10.1090/memo/0319.

Beckmann, P. (1973) *Orthogonal polynomials for engineers and physicists*. Golem Press.

Bonnet, J.P., Delville, J., Glauser, M.N., Antonia, R.A., Bisset, D.K., Cole, D.R., Fiedler, H.E., Garem, J.H., Hilberg, D., Jeong, J., Kevlahan, N.K.R., Ukeiley, L.S. and Vincendeau, E. (1998) 'Collaborative testing of eddy structure identification methods in free turbulent shear flows', *Experiments in Fluids*, 25(3), pp. 197–225. doi: 10.1007/s003480050224.

Cameron, R.H. and Martin, W.T. (1947) 'The Orthogonal development of non-linear Functionals in series of Fourier-Hermite Functionals', *The Annals of Mathematics*, 48(2), p. 385. doi: 10.2307/1969178.

Cassart, B., Teaca, B. and Carati, D. (2010) 'A general assessment method for subgrid-scale models in large-eddy simulation', *Physics of Fluids*, 22(10), p. 105105. doi: 10.1063/1.3495483.

Chen, Q.-Y., Gottlieb, D. and Hesthaven, J.S. (2005) 'Uncertainty analysis for the steady-state flows in a dual throat nozzle', *Journal of Computational Physics*, 204(1), pp. 378–398. doi: 10.1016/j.jcp.2004.10.019.

Chihara, T.S. (1978) *An introduction to Orthogonal polynomials (mathematics and its applications)*. New York: Harwood Academic (Medical, Reference and Social Sc.

Cools, R. (2003) 'An encyclopaedia of cubature formulas', *Journal of Complexity*, 19(3), pp. 445–453. doi: 10.1016/S0885-064X(03)00011-6.

Ferziger, J.H. and Peric, M. (2002). *Computational Methods for Fluid Dynamics*.

G., W. and Stroud, A.H. (1973) 'Approximate calculation of multiple integrals', *Mathematics of Computation*, 27(122), p. 437. doi: 10.2307/2005635.

Ghadiri Dehkordi, B. and Houri Jafari, H. (2009) 'Numerical simulation of flow through tube bundles in in-line square and general staggered arrangements', *International Journal of Numerical Methods for Heat & Fluid Flow*, 19(8), pp. 1038–1062. doi: 10.1108/09615530910994487.

Haber, S. (1970) 'Numerical evaluation of multiple integrals', *SIAM Review*, 12(4), pp. 481–526. doi: 10.1137/1012102.

Han, X., Sagaut, P., Lucor, D. and Afgan, I. (2012) 'Stochastic response of the laminar flow past a flat plate under uncertain inflow conditions', *International Journal of Computational Fluid Dynamics*, 26(2), pp. 101–117. doi: 10.1080/10618562.2012.655687.

Huerre, P. (1990) 'Local and global Instabilities in spatially developing flows', *Annual Review of Fluid Mechanics*, 22(1), pp. 473–537. doi: 10.1146/annurev.fluid.22.1.473.

Iacovides, H., Launder, B. and West, A. (2014). A comparison and assessment of approaches for modelling flow over in-line tube banks. *International Journal of Heat and Fluid Flow*, 49(C), pp.69–79.

Jayavel, S. and Tiwari, S. (2009) 'Numerical study of heat transfer and pressure drop for flow past inline and staggered tube bundles', *International Journal of Numerical Methods for Heat & Fluid Flow*, 19(8), pp. 931–949. doi: 10.1108/09615530910994432.

Kassera, V. and Strohmeier, K. (1997) 'Simulation of tube bundle vibrations induced by cross-flow', *Journal of Fluids and Structures*, 11(8), pp. 909–928. doi: 10.1006/jfls.1997.0114.

Kim, H.J. (1988) 'Investigation of the flow between a pair of circular cylinders in the flopping regime', *Journal of Fluid Mechanics*, 196(-1), p. 431. doi: 10.1017/s0022112088002769.

Kim, T. (2013). Effect of longitudinal pitch on convective heat transfer in crossflow over in-line tube banks. *Annals of Nuclear Energy*, 57, pp.209–215.

Lam, K. et al. (2003). Flow pattern and velocity field distribution of cross-flow around four cylinders in a square configuration at a low Reynolds number. *Journal of Fluids and Structures*, 17(5), pp.665–679.

Lam, K. and Fang, X. (1995). The effect of interference of four equispaced cylinders in cross flow on pressure and force coefficients. *Journal of Fluids and Structures*, 9(2), pp.195–214.

Le MaıˆtreOlivier and Knio, O.M. (2007) 'A stochastic particle-mesh scheme for uncertainty propagation in vortical flows', *Journal of Computational Physics*, 226(1), pp. 645–671. doi: 10.1016/j.jcp.2007.04.030.

Le Maî tre, O.P., Knio, O.M., Najm, H.N. and Ghanem, R.G. (2001) 'A stochastic projection method for fluid flow', *Journal of Computational Physics*, 173(2), pp. 481–511. doi: 10.1006/jcph.2001.6889.

Lucor, D., Meyers, J. and Sagaut, P. (2007) 'Sensitivity analysis of large-eddy simulations to subgrid-scale-model parametric uncertainty using polynomial chaos', *Journal of Fluid Mechanics*, 585, p. 255. doi: 10.1017/s0022112007006751.

Narayanan, V.A.B. and Zabaras, N. (2005) 'Variational multiscale stabilized FEM formulations for transport equations: Stochastic advection–diffusion and incompressible stochastic Navier–Stokes equations', *Journal of Computational Physics*, 202(1), pp. 94–133. doi: 10.1016/j.jcp.2004.06.019.

Ogura, H. (1972) 'Orthogonal functionals of the Poisson process', *IEEE Transactions on Information Theory*, 18(4), pp. 473–481. doi: 10.1109/tit.1972.1054856.

Patankar, S.V. and Spalding, D.B. (1972) 'A calculation procedure for heat, mass and momentum transfer in three-dimensional parabolic flows', *International Journal of Heat and Mass Transfer*, 15(10), pp. 1787–1806. doi: 10.1016/0017-9310(72)90054-3.

Puttock, J.S. and Hunt, J.C.R. (1979) 'Turbulent diffusion from sources near obstacles with separated wakes —part I. An eddy diffusivity model', *Atmospheric Environment (1967)*, 13(1), pp. 1–13. doi: 10.1016/0004-6981(79)90238-5.

Safwat Wilson, and Khalil Bassiouny, M. (2000). Modeling of heat transfer for flow across tube banks. *Chemical Engineering & Processing: Process Intensification*, 39, pp.1–14.

Sayers, A.T. (1988) 'Flow interference between four equispaced cylinders when subjected to a cross flow', *Journal of Wind Engineering and Industrial Aerodynamics*, 31(1), pp. 9–28. doi: 10.1016/0167-6105(88)90185-7.

Schoutens, W. (2000) *Stochastic processes and Orthogonal polynomials*. United States: Springer-Verlag New York.

Sumner, D., Wong, S.S.T., Price, S.J. and Paidoussis, M.P. (1999) 'Fluid behaviour of side-by-side circular cylinders in steady cross-flow', *Journal of Fluids and Structures*, 13(3), pp. 309–338. doi: 10.1006/jfls.1999.0205.

Traub, D. (1990). Turbulent heat transfer and pressure drop in plain tube bundles. *Chemical Engineering and Processing: Process Intensification*, 28(3), pp.173–181.

Weaver, D.S., Ziada, S., Sun, Z. and Feenstra, P. (2001) 'The effect of Platen fins on the flow-induced vibrations of an in-line tube array', *Journal of Pressure Vessel Technology*, 123(4), p. 437. doi: 10.1115/1.1408303.

West, A. (2013). Assessment of Computational Strategies for Modelling In-Line Tube Banks.

Xiu, D. (2010) *Numerical methods for stochastic computations: A spectral method approach*. United States: Princeton University Press.

Xiu, D. and Karniadakis, G.E. (2003) 'Modeling uncertainty in flow simulations via generalized polynomial chaos', *Journal of Computational Physics*, 187(1), pp. 137–167. doi: 10.1016/S0021-9991(03)00092-5.

Zdravkovich, M.M. and Stonebanks, K.L. (1990) 'Intrinsically nonuniform and metastableflow in and behind tube arrays', *Journal of Fluids and Structures*, 4(3), pp. 305–319. doi: 10.1016/s0889-9746(05)80017-9.

Zukauskas, A.A. (1972). Heat Transfer from Tubes in Cross Flow. *Advances in heat transfer, Academic Press*, 8, pp.93–106.

Gantt chart

Month	Feb.	Mar	Apr	May	June	July	Aug	Sept
Research Journals								
Writing gPC Pre Processor code in Fortran								
Grid Generation								
CFD simulations								
Writing gPC post Processor code in Fortran								
gPC - Validation								
CFD post processing								
gPC - Post processing								
gPC - results verification								
Report writing								
gPC - Literature survey								
gPC - validation								
Tube Bundles - Literature survey								
CFD - setup, turbulence modelling and numerical treatment								
Results and Discussion								
Conclusion								
Proof Reading								

Appendix A

This section supplies the plot of variation of mean coefficients of lift, drag and skin friction.

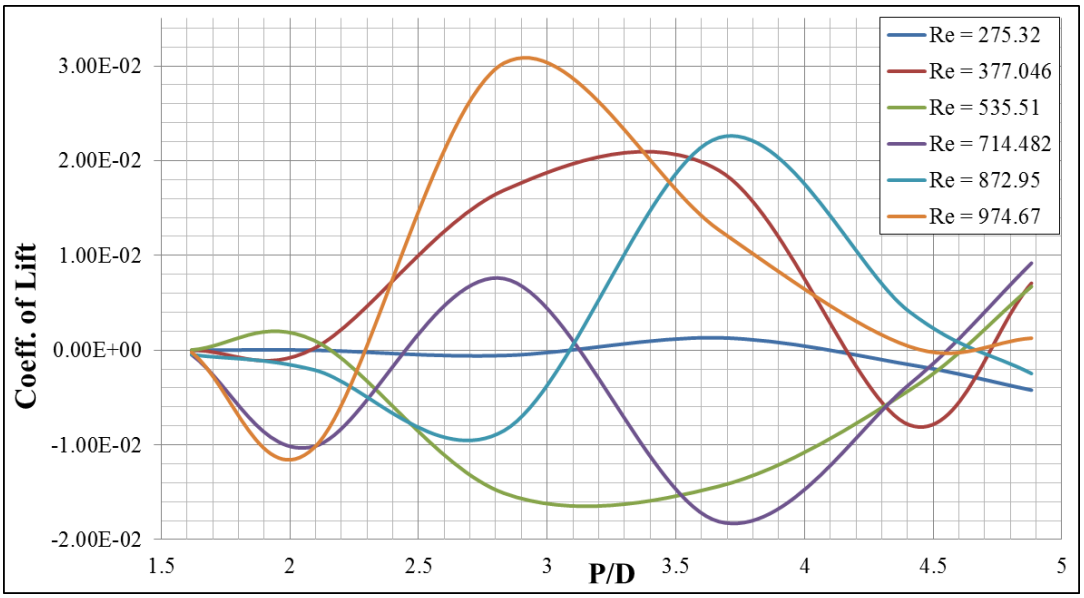

Figure 25: Plot of mean value of lift coefficient

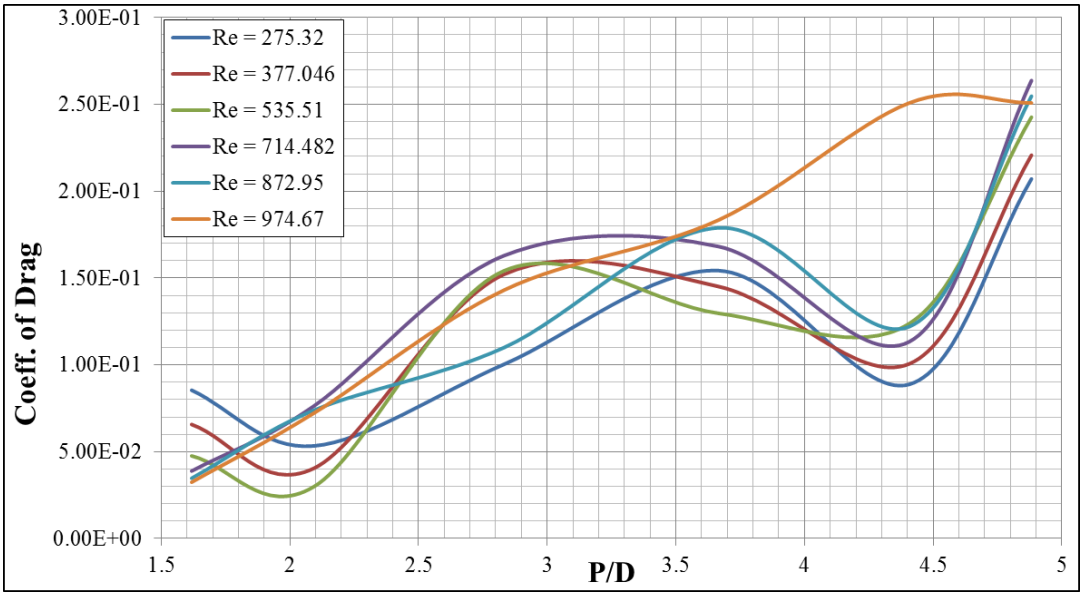

Figure 26: Plot of mean value of drag coefficient

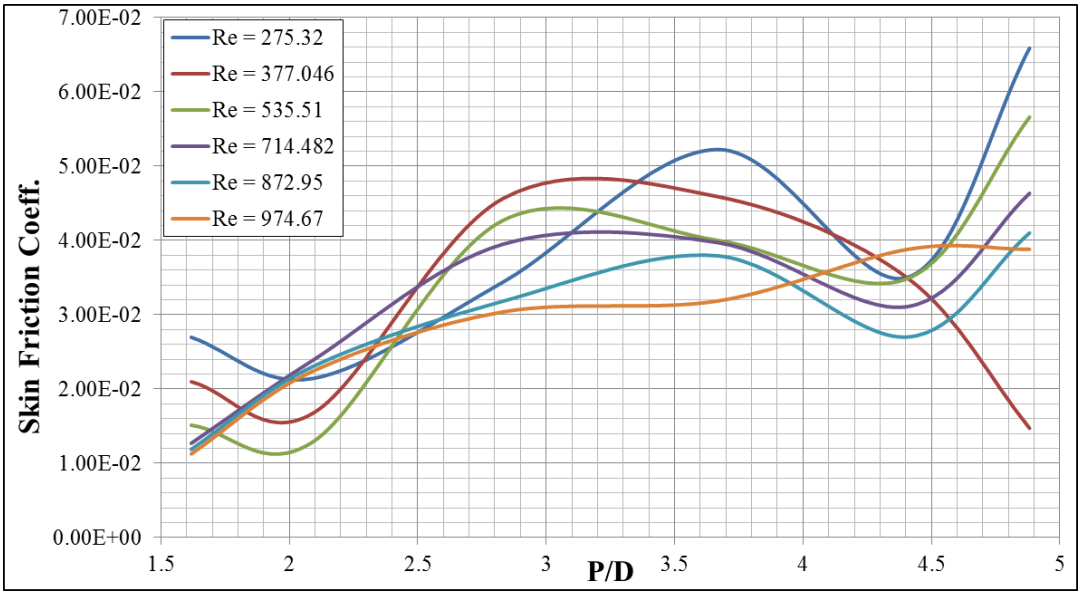

Figure 27: Plot of mean value of skin friction coefficient